

Wright State University

CORE Scholar

[Browse all Theses and Dissertations](#)

[Theses and Dissertations](#)

2014

Synthesis and Biological Activity of Indolinones

Kaleb Woodrow Cox
Wright State University

Follow this and additional works at: https://corescholar.libraries.wright.edu/etd_all

 Part of the [Chemistry Commons](#)

Repository Citation

Cox, Kaleb Woodrow, "Synthesis and Biological Activity of Indolinones" (2014). *Browse all Theses and Dissertations*. 1454.

https://corescholar.libraries.wright.edu/etd_all/1454

This Thesis is brought to you for free and open access by the Theses and Dissertations at CORE Scholar. It has been accepted for inclusion in Browse all Theses and Dissertations by an authorized administrator of CORE Scholar. For more information, please contact library-corescholar@wright.edu.

Synthesis and Biological Activity of Indolinones

**A thesis submitted in partial fulfillment
of the requirements for the degree of
Master of Science**

**By
KALEB WOODROW COX
B.S., Wilmington College, 2012**

**2014
Wright State University**

WRIGHT STATE UNIVERSITY
GRADUATE SCHOOL

December 18, 2014

I HEREBY RECOMMEND THAT THE THESIS PREPARED UNDER MY SUPERVISION BY Kaleb Woodrow Cox ENTITLED Synthesis and Biological Activity of Indolinones BE ACCEPTED IN PARTIAL FULFILLMENT OF THE REQUIREMENTS FOR THE DEGREE OF Master of Science.

Daniel Ketcha, Ph.D.
Thesis Director

David Grossie, Ph.D., Chair
Department of Chemistry
College of Science and
Mathematics

Committee on Final
Examination

Daniel Ketcha, Ph.D.

Eric Fossum, Ph.D.

Kenneth Turnbull, Ph.D.

Robert E. W. Fyffe, Ph.D.
Vice President for Research and
Dean, Graduate School

Abstract

Cox, Kaleb Woodrow. M.S., Department of Chemistry, Wright State University, 2014.
Synthesis and Biological Activity of Indolinones.

Indolinones of the type known as Arylidene oxindoles have been demonstrated to possess a broad range of activity ranging from protein kinase inhibitors, cell-death inhibitors and tau protein binding agents. Small libraries of such molecules were designed and synthesized herein in modifications involving variously substituted halogen derivatives, *N*-alkylation of the indolinone nitrogen, and finally a new class of molecules, namely arylidene oxindoles possessing extended conjugation. The biological activities of such molecules were examined and the results disclosed herein.

Table of Contents

	Page
I. Introduction.....	1
A. Statistics.....	2
B. Diagnosis.....	3
C. β-Amyloid Hypothesis.....	4
D. β-Amyloid Imaging.....	13
E. Tau Hypothesis.....	28
F. Small Molecules for Imaging Tau.....	30
G. Consideration of Benzylidene Oxindoles as Potential Tau Binding.....	39
H. PET and SPECT Imaging.....	41
II. Results and Discussion.....	42
A. Experimental.....	56
B. References.....	69

List of Figures

	Page
Figure 1: ^1H NMR of 1-Methyindolin-2,3-dione.....	47
Figure 2: ^1H NMR of 1-Methylindolin-2,3-dione from Sigma-Aldrich.....	47
Figure 3: Figure 3: ^1H NMR of 1-(2-Fluoroethyl)indol-2,3-dione.....	50

List of Tables

	Page
A. Table 1: 3-Substitued Indolin-2-ones from Knoevenagel Condensation.....	44
B. Table 2: 1-Methylindolin-2,3-dione.....	46
C. Table 3: <i>N</i> -Methyl Benzylidene Oxindoles.....	52
D. Table 4: Extended 3-Substitued Indolin-2-ones.....	56

Introduction

Alzheimer's disease (AD) is a condition with broad scientific, economic and social ramifications and has been the subject of 195,510 publications.¹ Alois Alzheimer first discovered a novel form of dementia when a patient named Auguste Deter came under his care while he was working at the Frankfurt Asylum in 1901.²⁻³ The first symptom exhibited by this patient was jealousy of her husband.² Soon after she began to experience rapid loss of memory and was disorientated in her own home, ultimately showing complete helplessness in the institution. Upon death, post-mortem examination of the brain showed an evenly atrophic brain without macroscopic focal degeneration and the larger vascular tissues (tissues containing blood vessels) showed arteriosclerotic change.² Alzheimer described Deter's disease as a progressive presenile dementia with general atrophy. These findings indicated that the patient had a neurodegenerative disease that was similar to Pick's disease in that both display bilateral degeneration of the cortical association areas which begin in the third and fourth decades.² Silver staining of the specimens showed changes in the neurofibrils.² Inside of a cell that looked completely normal were several fibrils that were distinguished by their unique thickness and capacity for impregnation.² With further examination, many fibrils were located next to each other, which have been changed in the same way by their thickness and capacity.² Next, they were observed at the surface of the cell combined in bundles.² Finally, the observation of the neurofibrils showed that the nucleus and the cell itself disintegrated and only a tangle of fibrils indicated the place where a neuron was previously located.² Alzheimer's first report on this patient was presented at the *37. Versammlung sudwestdeutscher Irrenarzte* (37th Meeting of the Southwest German Psychiatrists) in

Tubingen on November 3, 1906.²⁻³ Alois Alzheimer's second published case was about a 56-year old demented man named Johann F. who was admitted to the psychiatric clinic in 1907. When Johann F. died, neuropathological examinations of his brain showed an abundance of amyloid plaques but not a single neuron showed neurofibrillary change.⁵ Johann F.'s case was in slight contradiction with Deter's case, whose brain was autopsied and an abundance of both amyloid plaques and neurofibrillary tangles were observed.

It was hypothesized by some that Auguste Deter might have suffered from a different form of dementia.⁵ One hypothesis from Adamaccia implied that Deter had a rare disorder called metachromatic leukodystrophy which affects the growth of myelin,⁵⁻⁷ a fatty covering that protects and acts like an insulator around nerve fibers.⁷ As Alzheimer was familiar with metachromatic stains, this first hypothesis seems unlikely.⁵⁻⁷ A second hypothesis by O'Brien suggested that Deter might have suffered from arteriosclerosis, which is hardening of the arteries in the brain, causing Auguste's dementia.^{4,5}

Statistics

AD is the most common form of dementia and affects roughly 5.4 million people in the United States and 35 million people worldwide.⁸ Longer life expectancies in general and the aging of 76 million baby boomers will expectedly increase the numbers and percentages of Americans who will be among the oldest-old (85 yrs or older) of that generation. Between 2010 and 2050, the oldest old are expected to increase from 15% of all older people in the United States to one in every four older Americans (24%). This will result in an additional 15 million oldest-old people, individuals at risk for developing

AD. By 2050, the number of Americans age 85 and older will nearly quadruple to 21 million. In 2012, the population age 85 and older will include approximately 2.5 million people with AD, or 48% of the AD population age 65 and older. When the first wave of baby boomers reaches 85 in 2031, an estimated 3.5 million people aged 85 and older will have AD.⁸ As of 2012, someone in America will develop AD every 68 seconds and by the year 2050 someone in America will develop AD every 33 seconds. This will lead to nearly a million new cases per year, and AD prevalence is projected to be 11 million to 16 million at that time.⁸ At present, AD is the 6th leading cause of death in the United States and the 5th leading cause of death in Americans 65 and older.⁸ While the causes of death from other major causes are on the decline, AD has risen dramatically. Between 2000 and 2008, the proportion of deaths due to heart disease, stroke, and prostate cancer decreased by 13%, 20%, and 8%, respectively, whereas the proportion of deaths due to AD increased by 66%.⁸ Thus, the aging of the “baby boom” generation will increase the number of persons affected by the disease and place a huge burden on such patients, their caregivers, and society.⁹ This can cause an exponential amount of dollars to be spent on the healthcare needs of these patients and cause a huge burden on the people taking care of them.

Diagnosis

Although, there is no way to prevent, slow down, or cure AD, the disease can be characterized through various pathological biological markers in the brain. These pathological markers mainly consist of large numbers of amyloid plaques surrounded by neurons containing neurofibrillary tangles, also accompanied by vascular damage from

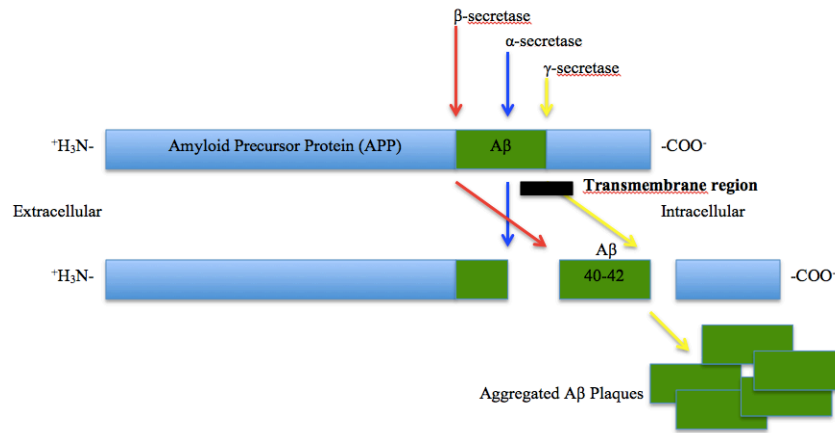
extensive plaque deposition, and neuronal cell loss.¹⁰ It is unknown whether amyloid or neurofibrillary tangles are the earliest lesions in the disease process, and thus the role of these markers in the etiology of the disease remains controversial.¹⁰

β -Amyloid Hypothesis

The strong association of amyloid plaques with AD has led to the so-called “amyloid hypothesis”, which suggests that amyloid β protein ($A\beta$) is the causative agent of Alzheimer’s pathology and that the neurofibrillary tangles, cell loss, vascular damage, and dementia follow as a direct result.¹⁰ Amyloid β is a peptide that results from processing of the amyloid precursor peptide (APP) and can be anywhere from 39 to 42 amino acids long.¹⁰ Amyloid precursor protein is an intermembrane peptide (inserted into the cytoplasmic membrane in the synapses of neurons) and is cleaved at residues 15 and 17 by enzymes called secretases to afford $A\beta$ fragments which then aggregate to form plaques.

The enzyme α -secretase cleaves APP within the $A\beta$ domain and thus precludes the generation of $A\beta$.¹¹ This cleavage yields secretory α -APPs that comprise most of the N-terminus ectodomain of APP, and the remaining membrane-bound C-terminal fragment (p3CT).¹¹ Alternatively, APP can also be cleaved by β -secretase, which cleaves APP at the N-terminus of $A\beta$, generating a truncated, soluble β -APP and a C-terminus fragment of 99 residues (A4CT, C99).¹¹ The β -secretase product A4CT contains the entire $A\beta$ domain, the transmembrane domain, and the cytoplasmic tail of APP, and represents the direct precursor protein.¹¹ Both membrane bound C-terminal fragments of APP (A4CT and p3CT) are cleaved by γ -secretase within their transmembrane domains

at the C-terminus of A β or p3.¹¹ This cleavage, catalyzed by γ -secretase, releases residual 40 and 42 A β fragments (A β_{40} and A β_{42}) with 40 being the most abundant and 42 being more neurotoxic and prone to aggregation. The disease state of AD is generally considered to be the result of an imbalance between A β production and clearance.¹²



Although the amyloid hypothesis offers a broad framework to explain AD pathogenesis, it is currently lacking in detail as to why it causes AD and certain clinical observations do not fit with the simplest version of the hypothesis.¹² Notably, the number of amyloid deposits in the brain does not correlate to the degree of cognitive impairment; additionally, some humans without symptoms of AD have appreciable deposits of A β .¹² A study by Wang *et al* used an enzyme-linked immunosorbent assay (ELISA) to compare soluble, insoluble, and total A β_{1-40} and A β_{1-42} in AD brains with those of age-matched normal and pathologic aging brains.¹³ There were a total of 43 participants studied: 23 brains from AD patients (age range of 69-91; average age of 81); 10 pathologic aging brains from subjects without clinical evidence of dementia including 4 subjects who were documented to be free of cognitive impairments prior to death by serial neuropsychological examinations (age range of 67-98; average age of 87) and 10 brains

with rare or no AD lesions from elderly individuals without clinical evidence of a neurological illness (age range of 60-93; average age of 73).¹³ The ELISA showed that there was a statistically significant increase (20-fold) in the average levels of total $A\beta_{1-40}$ in the AD brains compared to the pathologic aging brains ($P < 0.003$), and the observed 2-fold increase in the average levels of total $A\beta_{1-42/43}$ in the AD brains also was statistically significant ($P < 0.001$) compared to the average levels of this $A\beta$ peptide in the pathologic aging brains.¹³ The soluble pools of $A\beta_{1-40}$ and $A\beta_{1-42}$ were the largest total fractions of $A\beta$ in the normal brain (50 and 23%). These soluble pools were the lowest in AD brain (2.7 and 0.7 %) and the pathological brain was intermediate at 8 and 0.8 %.¹³ The data on soluble and insoluble $A\beta_{1-40}$ and $A\beta_{1-42/43}$ in pathologic aging suggest that this condition may reflect a transition state between the normal aging and the AD brain.¹³ However, the species of $A\beta$ in the pathologic aging specimens have not been extensively characterized and it is likely that these brains accumulate other $A\beta$ species, including those found in normal and AD brains.¹³ These findings could suggest that $A\beta$ could not be the cause of AD.

Another major factor in the amyloid hypothesis is the genetic evidence that the AD-causing mutations in APP, presenilin 1 and presenilin 2 (PS1 and PS2), increase the production of $A\beta$, causing early-onset or familial Alzheimer's disease (FAD).¹² A study by Citron *et al* used transfected cell lines and transgenic mice to determine $A\beta$ production from PS1 and PS2 mutations. For the transfected cell lines they used 293 kidney cells expressing APP₆₉₅ carrying the Swedish APP mutation¹⁴, which is known to make a better substrate for β -secretase, thereby increasing production of $A\beta_{40}$ and $A\beta_{42}$. They then transfected the mutant APP with PS1 or PS2, and this cell line was chosen for the PS

transfection because its high total A β secretion allows an accurate quantification of A β ₄₂ by (ELISA).¹⁴ For the transgenic mice study, Citron *et al* bred mice bearing wild-type human APP₆₉₅ gene with mice bearing human PS1 transgene.¹⁴ These mice would produce offspring expressing wild human-type APP₆₉₅ alone (single-transgenic mice) or both wild type APP₆₉₅ and either mutant or wild-type human PS1 (double-transgenic mice).¹⁴ The degree to which particle mutation affects A β production in cell cultures showed no correlation to which symptoms start to first appear.¹⁴ This strategy was chosen because endogenous mouse APP is not associated with human A β production under physiological or naturally occurring pathological conditions.¹⁴ Additionally, use of the same promoter element for both transgenes offers the advantage that both are likely to be expressed in adequate quantities in the same cell.¹⁴ The combined *in vitro* and *in vivo* data demonstrated that FAD-linked presenilin mutations directly or indirectly alter the activity of γ -secretase, but not α - or β -secretase, resulting in increased proteolysis of APP at the A β site and heightened A β ₄₂ production.¹⁴ The biological mechanism of this effect is presently unknown.¹⁴ The correlation between the size of the effect on APP processing and the age of onset of disease assessed in families with the mutations was not informative.¹⁵ Some PS mutations that strongly increase A β production seem to be associated more with special symptoms such as spastic paraparesis, a disease causing weakness affecting the lower extremities, and the occurrence of large “cotton wool” plaques,^{12,16,17} rather than those with early onset AD.^{12,16,17} Cell cultured models of AD have shown that the A β -elevating effects of PS mutations are similar to those of the COOH-terminal of APP mutations; however, the age at which symptoms appear in the latter cases but not the former, is accelerated by inheritance of apolipoprotein E (apoE4)

alleles.^{12,18} The reason for these phenotype discrepancies are unclear, but they may relate to the fact that cell culture systems do not adequately reflect the complexity of A β economy in the human brain.¹²

The amyloid hypothesis is still controversial because a specific neurotoxic species of A β and how it affects neuronal function have not yet been studied *in vivo*.¹² Another concern with the amyloid hypothesis is that transgenic mice undergoing progressive A β deposition^{19,20} often do not show clear-cut neuronal loss.²¹ The reasons for the failure of mice expressing only an APP transgene to show neurofibrillary degeneration and substantial neuronal loss are not yet clear but there are several plausible explanations.¹² For instance, each species of mice can have different neuronal vulnerabilities, the absence of human tau molecule in these mice, the lack of a full complement of human-type inflammation mediators (certain cytokines) and the relatively short exposure to A β could also be a reason why these mice show no neuronal loss.¹² The finding that an APP transgene clearly accelerates neurofibrillary tangle formation in APP/tau double-transgenic mice²² suggests a causal connection between A β accumulation and neurofibrillary degeneration, even in mouse models.¹²

Another criticism to the amyloid hypothesis was based upon the work of Braak and Braak²³ who showed that neurofibrillary degeneration of cell bodies increases gradually with the age of humans and that these changes predate morphologically detectable amyloid plaques. However, the earliest cases examined in these postmortem studies were actually nondemented older individuals, and it is impossible to know

whether their neurofibrillary changes represented the prodrome, or early symptoms of AD.^{12,23}

The amyloid hypothesis also has discrepancies on whether or not A β plaques cause AD.¹² Patients with Down's syndrome, who also have dementia and have an abundance of A β plaques and NFTs, also have died at varying ages where A β deposition predates neurofibrillary tangle formation.^{12,24,25} Also, an Australian family had a spastic paraparesis variant of familial AD. When an individual family member died of unrelated causes, she died after the onset of the paraparesis but before the onset of dementia.¹⁷ During a neuropathological examination, fulminant amyloid deposition was present but no neurofibrillary tangles.¹⁷ The patient showed altered APP processing and A β accumulation clearly predated tau changes and neuronal injury.¹⁷ This indicated that the patient had A β plaques but did not have dementia. Another indication that might suggest that A β is not the leading causing in AD is the clinical failures of two amyloid antibodies solanezumab and bapineuzumab. These two antibody drugs were design to slow the decline in memory, cognitive decline, and performance of activities of daily living and personal care.²⁷ The antibodies point of attack was to reduce brain amyloid load either by reducing soluble amyloid in the fluids, decreasing accumulation of plaques, or by increasing plaque clearance through immunogenic microglial activation.²⁷

Solanezumab was compared with a placebo in two trials involving a total of 2,052 patients with mild-to-moderate Alzheimer's disease.²⁶ The patients were given either 400 mg of Solanezumab or a placebo intravenously ever 4 to 18 weeks.²⁶ The primary outcomes were measured from the changes of the baseline to the end of the study on the

11-item cognitive scale the Alzheimer's Disease Assessment Scale (ADAS-cog11) with scores from 0 to 70 and higher scores indicating more impairment and the Alzheimer's Disease Cooperative Study-Activities of Daily Living scale (ADCS-ADL) with a range of 0 to 78 with lower scores indicative of poorer functioning.²⁶ The first trial was called EXPEDITION 1 and after the first trial's data was analyzed, the EXPEDITION 2 trial was revised to include changes in scores of a 14-item ADAS-cog14 in patients with mild disease, which is thought to be more relevant for assessing people with earlier-stage Alzheimer's.²⁶ The researchers concluded that "none of the first trials for Solanezumab showed any significant improvement in the primary outcomes and that studies failed to show treatment effects on the hippocampal or total brain volumes or on amyloid accumulation on the PET scan."²⁶

However, there were some positive signs for Solanezumab. For example, the measures of biomarkers, including plasma cerebrospinal fluid (CSF) levels of antibody, are consistent with the target engagement of soluble brain amyloid.²⁶ The edema, 0.9 percent compared with 0.4 percent, among the drug treatment group compared with placebo, and hemorrhage rates were 4.9 percent and 5.6 percent respectively.²⁶ About 25 percent of participants with mild disease tested negative for amyloid on PET imaging, meaning they likely had another type of dementia rather than Alzheimer's.²⁶ Dr. Eric Karren and Dr. John Hardy stated, "in EXPEDITION 3, positivity on PET amyloid is an inclusion criteria, and this will greatly increase the potential to show efficacy."²⁶

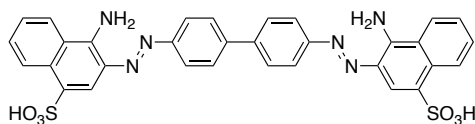
Bapineuzumab was tested in two phase 3 multicenter trials of patients with mild-to-moderate Alzheimer's disease.²⁶ There were 1,121 patients who were carriers of the

APOE4 gene, which is associated with a higher risk of Alzheimer's disease, and 1,331 patients who were non-carriers were treated.²⁶ For every 13 weeks for 78 weeks, patients were given an intravenous dose of Bapineuzumab or a placebo with dosage depending on body weight.²⁶ The primary outcomes were measured on ADAS-cog11 scores and the Disabilities Assessment for Dementia (DAD).²⁶ The DAD scores were from 0 to 100 with higher scores meaning less impairment.²⁶ Baseline measurements were compared at the end of the 78 weeks trial. The measurements for the secondary outcomes were based on the findings of PET imaging and the cerebrospinal fluid phosphorylated tau (phosphor-tau) concentrations.²⁶ The researchers reported that there were “no significant differences between the Bapineuzumab groups and the placebo groups with respect to primary endpoints.”²⁶ The major safety findings were amyloid-related imaging abnormalities with edema among patients receiving those in higher doses and APOE carriers.²⁶ In the secondary outcome measures, the study found a reduction in phosphor-tau concentrations in the spinal fluid of APOE carriers.²⁶ Researchers believe this may be an indication that less neurodegeneration was occurring.²⁶ PET scans also showed that patients receiving the drug showed less evidence of amyloid buildup.²⁶ Dr. Salloway stated that both of the findings suggest that the antibody therapy was having some effect on amyloid, even if the clinical benefit was not apparent and the antibody treatment might work better at an earlier stage of Alzheimer's.²⁶ Researchers conducting the study wrote, “amyloid accumulation probably starts many years before the onset of symptoms, and anti-amyloid treatment only after dementia develops may be too late to affect the clinical course of the disease.”²⁶

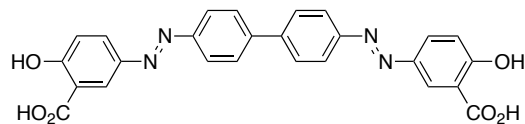
Norman Relkin, associate professor of neurology at Weill Cornell Medical College told *Neurology today* that there were nuances in the findings that need to be considered.²⁶ Relkin suggested the results need to be considered for the overall negative findings in context, stating: “The results don’t mean that there is not a future role for immunotherapy for treating AD and they do not mean that amyloid is not a therapeutic target. The challenge is to find the right drug, the right timing, the right dose.” Rachele S. Doody, professor of neurology and director of the Alzheimer’s Disease and Memory Disorders Center at Baylor College of Medicine, and the lead author of the report on solanezumab, said that the negative results in the primary outcomes indicate that the drug should not be approved as a treatment for mild-to-moderate Alzheimer’s disease.²⁶ She also felt that a secondary analysis of the data suggest that Solanezumab could be useful for those with mild disease.²⁶ The drug is currently under way in three trials to test for either mild or asymptomatic disease. The study on mild disease involves people with sporadic AD and the asymptomatic studies are in carriers of mutations for familial AD and in people who have positive amyloid scans.²⁶ Doody suggested that future research aimed at studying therapies in people with mild or asymptomatic diseases needs to occur alongside the development of new drugs for people with the full-blown illness.²⁶ Doody noted that the two drugs that targeted amyloid worked in different ways. Bapineuzumab binds to aggregated amyloid beta, including plaques,²⁶ whereas solanezumab binds to soluble amyloid beta.²⁶

β-Amyloid Imaging

There have been many approaches for imaging β -amyloid. The earliest of these involved using conjugated dyes for post-mortem staining of the brain. Congo red (**1**) is a dye that can bind to $A\beta$, but also binds to a whole array of molecules held in proper orientation by virtue of the beta-sheet fibril.²⁷ Congo red not only binds to β -amyloid, but to tau protein as well.²⁷ However, Congo red is not very lipophilic due to it having a positive and negative charge at both ends which precludes its ability to cross the blood brain barrier (BBB).²⁷ To modify the lipophilicity of this structure and enhance its ability to cross the BBB, Klunk and coworkers at the University of Pittsburgh synthesized Chrysamine G (CG) **2**.²⁷ CG has hydroxyl and carboxylic acid groups on both ends which makes it neutral and allows it to cross the BBB in mice and a lower inhibition constant (K_i).²⁷ The K_i value measures the concentration of the inhibitor that is required in order to decrease the maximal rate of reaction itself. The higher K_i value, then the more concentration of ligand is required. For the inhibition of radiolabeled [¹⁴C]**2** binding to $A\beta(1-43)$ had an inhibition K_i of $0.43 \pm 0.12 \mu\text{M}$ compared to CR, while CR had a K_i of $2.82 \pm 0.84 \mu\text{M}$.²⁷

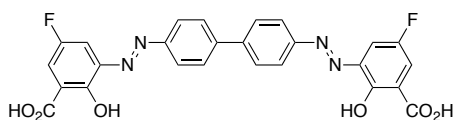


1

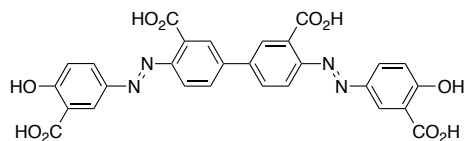


2

The K_i for the inhibition of [¹⁴C]**2** binding to $A\beta(1-43)$ was also done for the analogues of **2** shown below. The difluoro derivative **3** of CG was only slightly less potent than CG itself ($K_i = 1.6 \mu\text{M} \pm 0.19$), while the 3,3'-dicarboxylic acid derivative **4** had a similar K_i value to Congo Red ($2.76 \pm 0.52 \mu\text{M}$).²⁷

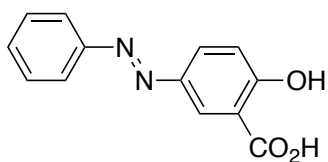


3

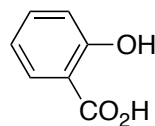


4

In an attempt to explore the importance of the bidentate nature of the functional groups of CG, Klunk *et al.* studied the binding of the diazo derivative **5**, which represents one-half of a CG molecule. An approximation of the energy of binding can be calculated by using the value of 0.43 μM for the K_i of CG, the energy of binding is roughly 36 KJ/mole. If the diazo derivative binds with half of this energy, the expected binding energy would be about 18,000 J/mole. The derivative **5** has a K_i of 73 ± 54 and the binding energy is $23,000 \pm 17,500$ J/mole, which is in agreement with the predicted value. The importance of the hydrophobic region of CG and the aniline derivative is demonstrated by the lack of binding of salicylic acid (**6**) itself.²⁷



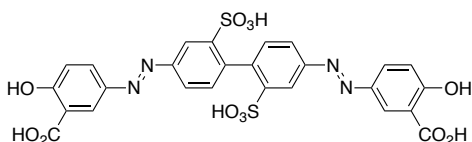
5



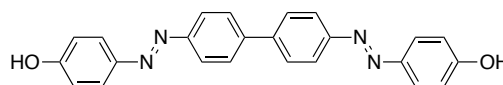
6

Another derivative of CG that was inactive was the 2,2'-disulfonic acid derivative **7**. Since the compound **4** showed little loss of activity from CG, it is unlikely that the additional acid moieties are the sole cause for the loss of activity in **7**. Presumably, the bulky sulfonate groups in the 2-position force the biphenyl group out of planarity.

Molecular modeling studies showed that the dihedral angle between the two-biphenyl benzene rings in **7** is 83° . This angle is approximately 35° in CG and all of the other active derivatives. The phenol derivative **8** is inactive, but gives important structure activity information. Since this derivative is identical to CG except for the carboxylic acid groups, the inactivity of the compound suggests that the acid moieties are essential for binding.²⁷

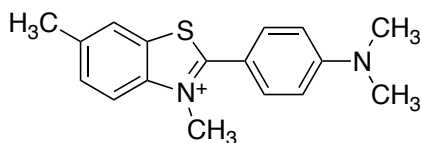


7

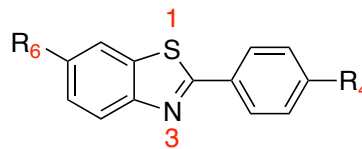


8

Another dye that is known to stain beta-amyloid post-mortem is Thioflavin-T (**9**), which also has an affinity for tau protein.²⁸ Since Thioflavin-T is a salt and unable to cross the BBB, in order to make Thioflavin-T more lipophilic Klunk synthesized 18 neutral 2-arylbenzothiazoles (BTA) **10** derivatives of thioflavin-T, substituting on the R₆ and R_{4'} positions.²⁸



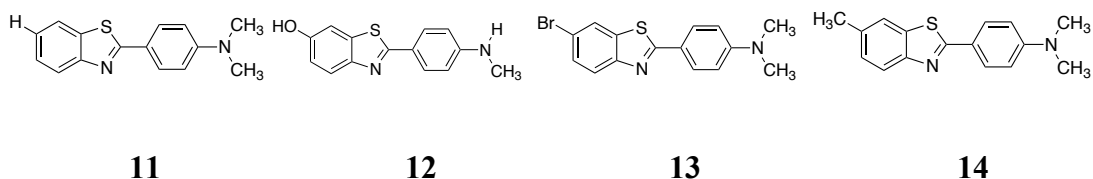
9



10

Amongst these benzothiazoles was BTA-1 (**11**) and 6-OH-BTA-1 (**12**), also known as Pittsburgh Compound-B (PIB). In a test of brain entry levels, BTA-1 with a carbon-11 radiolabel showed the highest brain entry with a value of 0.43 (%ID-kg)/g,

where (%ID-kg)/g is the percent injected dose per gram of brain (%ID/g) normalized to body weight (in kg).²⁸ The highly lipophilic derivatives 6-Br-BTA-2 (**13**) and 6-Me-BTA-2 (**14**) showed the poorest brain entry with (%ID-kg)/g values of only 0.054 and 0.078, respectively.²⁸ This may be a result of the phenomenon of blood element binding by highly lipophilic compounds ($\log P > 3$) where logP is the partition coefficient.²⁹ The 2-minute brain level of the BTA derivatives studied showed the classic parabolic relationship with $\log P_{C18}$. Radiolabelled BTA-1 was the only compound that didn't appear to fit a parabolic-type relationship. This demonstrates a considerably higher brain entry than any of the 12 other ¹¹C-labeled BTA derivatives.²⁸

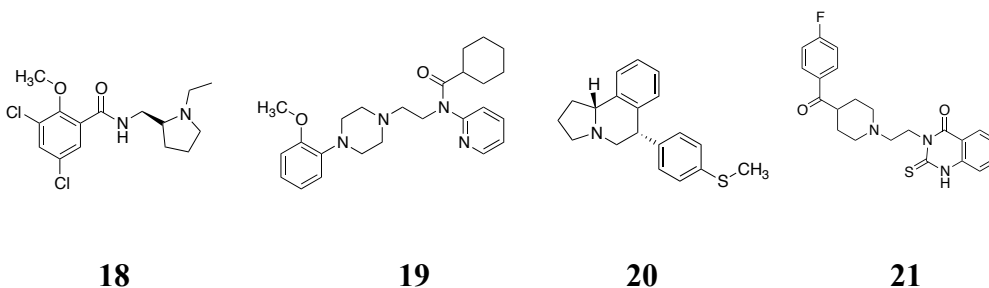


The radiolabeled derivatives were also tested for brain penetration in young, wild type Swish-Webster mice that had no amyloid deposits in their brain.²⁸ This study reflects brain entry and clearance from normal brain tissue.²⁸ A necessary criterion for a good PET imaging agent is rapid clearance from brain areas that do not contain the targeted binding site.²⁸ This is especially essential for short-lived ¹¹C-labeled radioligands. The (%ID-kg)/g values of the BTA derivatives showed that all but the two most lipophilic compounds, **13** and **14**, provided lower 30 min. brain values than 2 min.²⁸ The compound with the lowest 30 min. brain value (%ID-kg)/g value was **12**, with a more than 3-fold lower concentration than any other derivative.²⁸

is no myelin. Locations of gray matter include the cerebral cortex and basal nuclei. White matter is located between the brain stem and cerebellum and surrounds the nuclei. White matter is formed by axons of neurons and is white because of myelin. The regional heterogeneity of radioactivity concentrations was greater for BTA-1 than it was for 6-OH-BTA-1, and the pons was particularly evaluated for BTA-1 because of higher concentrations of radioactivity. The concentration of radioactivity in baboon cortex was nearly identical to that in the cerebellar cortex at all time points for all of the derivatives studies.²⁸

The maximum brain radioactivity concentration (%ID-kg)/g in baboons correlated significantly with 2 min (%ID-kg)/g values in mice ($r = 0.85$), with maximum brain concentration of radioactivity resulting from BTA-1 > 6-MeO-BTA-1 > 6-CN-BTA-1 > 6-Me-BTA-1 > 6-OH-BTA-1.²⁸ Brain radioactivity concentrations of BTA-1 and 6-OH-BTA-1 were remarkably similar in mice and baboons (0.43 vs. 0.45 for BTA-1 and 0.21 vs. 0.27 for 6-OH-BTA-1).²⁸ Compared to the mouse brain, the clearance of radioactivity was considerably slower for the baboon brain, although the rank order of clearance rate was similar in mice and baboons with 6-OH-BTA-1 being the fastest and 6-Me-BTA-1 being the slowest clearing derivative.²⁸ Monoexponential fits of radioactivity loss from baboon cortices resulted in the following clearance half-times ($t_{1/2}$ values): 6-Me-BTA-1 = 111 min, 6-MeO-BTA-1 = 55 min, 6-CN-BTA-1 = 51 min, BTA-1 = 20 min, and 6-OH-BTA-1 = 13 min.²⁸ As in the mice studies, 6-OH-BTA-1 and BTA-1 resulted in the highest ratios of early-to-late brain radioactivity concentrations in baboons (4.6 and 2.8 respectively).²⁸

Comparison of the *in vivo* behavior of the two lead compounds (6-OH-BTA-1 and BTA-1), in baboon brain to that of the entry and clearance of other successful PET radioligands in a reference brain region devoid of specific binding sites, like the cerebellum, was helpful in selecting the lead ^{11}C -labeled BTA derivative to take into human studies.²⁸ Klunk *et al* compared 6-OH-BTA-1 and BTA-1 to 4 compounds: [^{11}C]raclopride **18**, [carbonyl- ^{11}C]WAY100635 **19**, [^{11}C](+)-McN5652 **20**, and [^{18}F]altanserin **21**.²⁸



The relatively rapid nonspecific binding clearance rates of [carbonyl- ^{11}C]WAY100635, [^{11}C] raclopride, and [^{18}F] altanserin are important in the success of these PET radioligands for imaging the serotonin 5-HT_{1A}, dopamine D₂, and serotonin 5-HT_{2A} receptor systems.³⁰⁻³⁵ In contrast, the relatively slow *in vivo* clearance of [^{11}C](+)-McN5652 has limited the usefulness of this radioligand for imaging the serotonin transporter system.^{36,38} The ^{11}C -labeled BTA compounds with similar rapid nonspecific binding clearance properties within the range bracketed by [carbonyl- ^{11}C]WAY100635 and [^{18}F]altanserin might prove useful as an *in vivo* imaging agent for amyloid plaques.²⁸

The brain clearance properties of [^{11}C]6-OH-BTA-1 indicated that the relatively rapid rate of nonspecific clearance of this radiotracer ($t_{1/2} = 13$ min) was similar to that of other useful PET neuroreceptor imaging agents while those of [^{11}C]BTA-1 ($t_{1/2} = 20$ min)

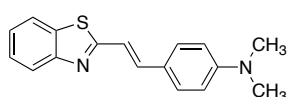
were too slow.²⁸ From this study, it was only possible to critically assess the rates of *in vivo* clearance of the free and nonspecifically bound radioactively ¹¹C-labeled BTA derivatives in the brains of rodent and nonhuman primate animal models.²⁸

As a qualitative measure of specificity for amyloid deposits, nonradiolabeled (cold) 6-OH-BTA-1 was used to stain paraffin sections of postmortem AD brain.²⁸ Like thioflavin-T, nearly all of the BTA derivatives are fluorescent compounds, and the staining of 6-OH-BTA-1 was localized to both A β plaques and cerebrovascular amyloid (CVA) in frontal cortex.²⁸ The identity of the plaques and CVA stained by 6-OH-BTA-1 was confirmed by staining serial sections with an antibody to A β . A β plaques and CVA are both composed predominantly of A β peptides.²⁸ The overall encouraging *in vitro* and *in vivo* properties of [¹¹C]6-OH-BTA-1, or Pittsburgh Compound-B (PIB) led to the choice of this agent for further evaluation in human subjects.²⁸

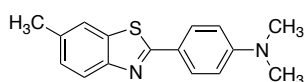
Klunk *et al* studied amyloid imaging with PET in humans with PIB. In the study, 25 patients, 16 with diagnosed mild AD and 9 controls, were compared. The AD patients typically showed marked retention of PIB in areas of association cortex known to contain large amounts of amyloid deposits in AD. The association cortexes consisted of the frontal, parietal, occipital, temporal, and cerebellar cortices, while the striatum, pons, and subcortical white matter were also investigated. In the AD group, PIB retention was increased most prominently in the frontal cortex (1.94-fold, $p = 0.0001$).³⁹ Large increases also were observed in parietal (1.71-fold, $p = 0.0002$), temporal (1.52-fold, $p = 0.002$), and occipital (1.52-fold, $p = 0.002$) cortices and the striatum (1.76-fold, $p = 0.0001$).³⁹ PIB retention was equivalent in AD patients and controls in areas known to be

relatively unaffected by amyloid deposition. These unaffected areas were the subcortical white matter, the pons, and cerebellum. The studies in three young (21 years) and six older healthy controls (69.5 ± 11 years) showed low PIB retention in cortical areas and no significant group differences between young and older controls.³⁹ In cortical areas, PIB retention correlated inversely with cerebral glucose metabolism as determined with ^{18}F -fluorodeoxyglucose.³⁹ This relationship was most robust in the parietal cortex ($r = -0.72$; $p = 0.0001$).³⁹ The results suggest that PET imaging with PIB can provide quantitative information on amyloid deposits in living subjects.³⁹ The drawback to using PIB is that it uses radiolabeled ^{11}C , which only has a half-life of 20 minutes. Using ^{11}C limits its use for facilities with an on-site cyclotron and a radiochemical team.⁴¹

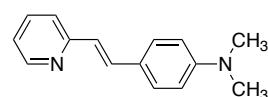
In 2001, Kung *et al.* synthesized a series of novel stilbenes as probes for amyloid plaques. To search for an $\text{A}\beta$ probe, Kung purchased a series of benzothiazole and stilbenes (SB) (**22-24**) from Sigma-Aldrich Chemical Company.



22

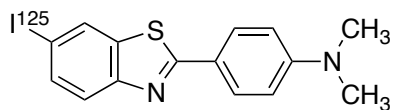


23

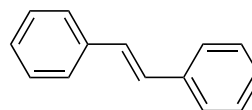


24

These three compounds were screened by *in vitro* binding assays. Two of the compounds (**22** and **23**) are analogues of TZDM (**25**), having the same benzothiazole core but the iodine is replaced with a -H or a -CH₃ and these derivatives showed strikingly high binding affinities for the benzothiazole (TZ) binding sites ($K_i = 2.3$ and 1.4 nM, respectively), while *E*-stilbenes **26** and **24** displayed low binding affinities ($K_i = 535$ and >1000 nM, respectively).⁴⁰

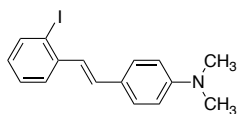


25

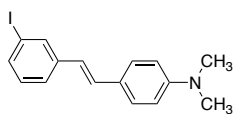


26

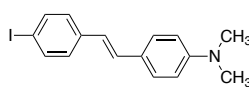
Based on these unexpected results, Kung et al. prepared and tested a series of stilbenes **27-32**, all of which contained an electron-donating group: *p*-Me₂N-, -OMe, or -OH.⁴⁰



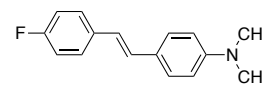
27



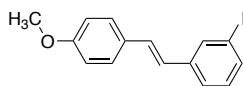
28



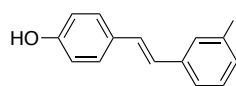
29



30



31



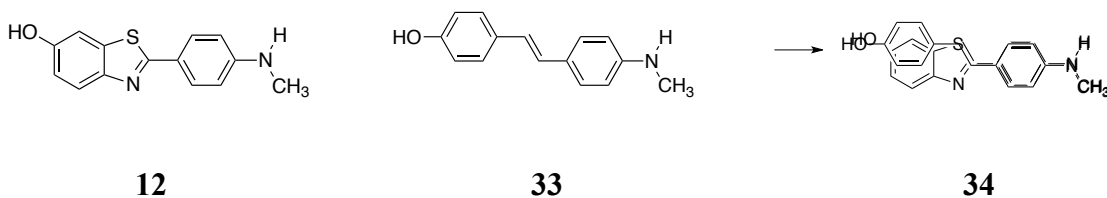
32

These stilbenes were prepared by a Wadsworth-Emmons reaction using diethyl phosphonates as the starting materials.⁴⁰ The in vitro binding assay used preformed A β aggregates of synthetic A β ₁₋₄₀ peptides and [¹²⁵I]TZDM as the ligand.⁴⁰ Stilbenes **27-32** showed high binding affinities ($K_i = 2-32$ nM) to the TZ sites, while affinities toward SB sites were very low (>1000 nM).⁴⁰ The binding affinity for the *p*-Me₂N-stilbenes is not sensitive to the position of the iodo group; *o*-, *m*-, or *p*-iodo substitutions (**27**, **28** or **29**) on one of the benzene rings of stilbene displayed about equal potency (2.0-7.7 nM).⁴⁰ The derivative **30** showed slightly lower affinity ($K_i = 22$ nM).⁴⁰ It is evident that these extremely simple and small stilbenes, containing an electron donating group such as *p*-

Me₂N-, -OMe, or -OH, displayed superb binding affinity to Aβ aggregates. Replacing the benzothiazole ring with an iodo- or fluoro-substituted phenyl ring had no effect on binding affinity at the TZ binding sites of Aβ aggregates.⁴⁰ Binding affinity appears to be determined by the pharmacophores on one side of the stilbene molecule (i.e., electron donating or withdrawing group), suggesting that additional modifications could be possible.⁴⁰

The stilbenes were further characterized with [¹²⁵I]28 as the radiotracer. An *in vivo* biodistribution studies of [¹²⁵I]28 in normal mice after iv injection suggested good brain penetration. The brain uptake was 0.72, 1.12, 1.08, and 0.19% dose/organ, and the brain/blood gram ratio was 0.46, 1.46, 1.34, and 0.24, at 2, 30, 60, and 240 min after injection. The blood levels were relatively low at 6.5-2.8% dose/organ at all of the time points.⁴⁰ Binding to the aggregates of Aβ₁₋₄₀ is saturable, and the dissociation constant (K_d) was 0.19 nM, which is similar to that observed for [¹²⁵I]TZDM.⁴⁰ The results suggest that molecular weight can be reduced while maintaining binding affinity; as such, it significantly enhances the flexibility on designing new probes for imaging Aβ plaques in the brain.⁴⁰ This finding is important, because it represents a structural simplicity and suggests better alternatives for designing probes for binding to Aβ aggregates: (1) these probes may contain a simple stilbene-like structure; (2) one of the aromatic rings contains an electron-donating group, *p*-Me₂N-, -OMe, or -OH, which appears to be essential for the binding affinity, and; (3) there is a bulk tolerance for the second aromatic ring, on which radiolabeled, ^{99m}Tc, ¹²³I, or ¹⁸F, can be readily attached without detrimental effects on binding affinity to Aβ aggregates.⁴⁰

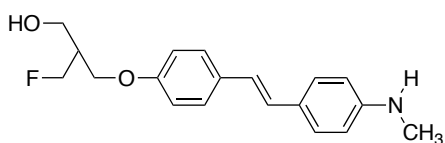
Kung et al. then recognized that the chemical structures of **12** and a stilbene derivative SB-13 (**33**) both have a highly conjugated aromatic ring system and are relatively planar molecules, which is an important attribute for insertion between the β -sheet of A β aggregates.⁴¹ Another common feature is an electron-donating group with a *N*-methylamino or a hydroxyl group at each end of the molecule.⁴⁰ The similar structures of **12** vs **33** (overlay structure **34**) appear to compete for similar binding sites on the A β aggregates.⁴¹ Structure **34** demonstrates overlap of the aromatic rings and the electron donating groups (e.g., *N*-methylamino and hydroxyl). In addition, both ligands are relatively planar because of the conjugated systems.



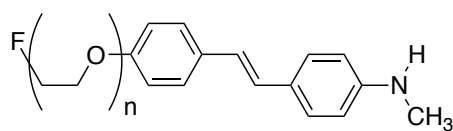
The rigid structures of stilbene and styrylpyridine provide the basic core structures for developing specific imaging agents for A β plaques.^{42,43} The stilbene derivative **33** showed excellent binding affinity to post-mortem AD brain tissue homogenates ($K_d = 2.4 \pm 0.2$ nM). *In vivo* human PET imaging studies with [¹¹C]**33** demonstrated potential usefulness in detecting A β plaques in the brain.⁴¹ To further improve the availability of ¹⁸F labeled PET imaging agents as a tool for diagnosis of AD, a series of fluorinated stilbenes were synthesized and tested.⁴¹ Adding a fluorine atom to the side chain for labeling while maintaining the desired binding affinity to A β plaques and brain penetrability was not a simple exercise. Initial attempts at developing ¹⁸F labeled **33** by adding a fluoroalkyl substituent group on either end of the stilbene core

met with little success.⁴¹ The stilbene derivatives were too lipophilic and showed high nonspecific binding in normal brain.

To reduce the lipophilicity of the stilbenes, two approaches were employed to develop ¹⁸F labeled PET imaging agents.^{42,43} Of these approaches, one involved the use of a 2-fluoromethyl-1,3-propylenediol group (e.g., as in **35**) and another employed a fluoro-pegylated (FPEG) group at one end of the phenol group (e.g., as in **36**).



35



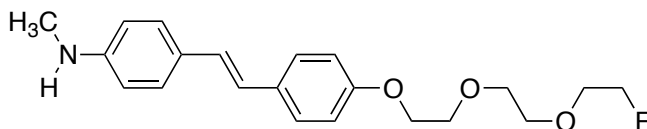
36

Among these two compounds, **35** displayed a high binding affinity in post-mortem AD brain homogenates ($K_i = 5.0 \pm 1.2$ nM),⁴¹ and was successfully labeled with ¹⁸F to produce [¹⁸F]**35**. The radiotracer was neutral and lipophilic and showed a moderate log *P* of 2.95.⁴¹ *In vivo* biodistribution of radiolabeled **35** in normal mice exhibited excellent brain penetration and rapid washout after an iv injection (4.66 and 0.33% dose/g in the brain at 2 and 60 min post injection, respectively).⁴¹ Excellent brain penetration and rapid washout are highly desirable for *Aβ* plaque-specific brain imaging agents. However, compound **35** has a fluorine containing side chain that has an optical center which might complicate *in vivo* metabolism.⁴¹

For a compound that does not have an optical center, a stilbene containing a FPEG group would be more appropriate.⁴²⁻⁴⁴ The FPEG linker on **33** helps modulate lipophilicity, maintain neutrality, and provides a simple nucleophilic substitution

mechanism for a labeling site with ^{18}F .⁴⁴ To modulate the lipophilicity of ^{18}F labeled stilbene **36**, different chain lengths of ethylene glycol (PEG, $n=2-12$) were added and the end of the chain was capped with a fluorine atom.^{43,44} The FPEG derivative **36** displayed excellent $A\beta$ -binding affinities and high brain penetration.⁴¹ Structure-binding studies of FPEG linkers showed that for chain lengths up to $n=8$, the K_i was $<10\text{ nM}$.⁴¹ The lipophilicity does not change greatly between $\log P$ of 2-3, however; the *in vivo* biodistribution studies in normal mice showed that when $n > 5$, there was a dramatic drop-off in brain penetration.⁴¹ These findings are unexpected because the molecular weight for **36** ($n=6$) is 490, which is below the commonly accepted cut-off point of 600 for penetration of intact BBB.²⁹ It is likely that molecular size is only one of the factors controlling brain penetration of small and neutral molecules.⁴⁵ The flexible and polar FPEG chain can also interfere and limit brain penetration.⁴¹

Based on its structure-activity characteristics, neutrality, and lipophilicity, **36**, with a PEG length of 3, was chosen to go on to further testing.⁴¹ This ligand is equivalent to BAY 94-9172 (AV-1, **37**), which was reported as a useful *in vivo* imaging agent for targeting $A\beta$ plaques in the living human brain.⁴⁶



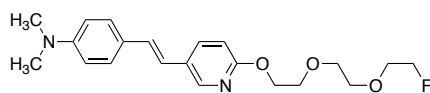
37

Compound **37** provides an excellent combination of *in vitro* and *in vivo* properties for $A\beta$ plaque labeling, which constitute desirable characteristics suitable for *in vivo*

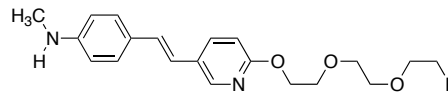
imaging agents.⁴¹ These properties include: (1) high in vitro binding affinity ($K_i < 10$ nM); (2) in vitro labeling of post-mortem human brain tissue sections displaying excellent labeling of A β plaque; (3) very high in vivo brain penetration and fast washout from normal brain regions; (4) high ex vivo labeling of A β plaque labeling in transgenic mice and excellent PET images in normal primate brain (high penetration and fast washout from normal regions); (5) low toxicity in normal animal models, and; (6) efficient ^{18}F labeling procedure adaptable for automated synthesis of PET tracers under a cGMP manufacturing condition.⁴¹ This last property is important because the half-life of ^{18}F is 110 min, which means there is a time-constraint on making the final drug product for regional distribution.⁴¹ Compound **37** was reported as a useful in vivo imaging agent for targeting A β plaques in living humans.⁴⁶ The preliminary clinical data indicated that **37** showed great promise as a PET imaging agent for detecting A β plaques in the living human brain.⁴¹ The optimal signal-to-noise ratio of **37** was reached at 70-90 min after iv injection.⁴¹

With this information, it was found that adding a styrylpyridine to the ring reduced lipophilicity even further.⁴¹ From a series of styrylpyridines, AV-19 (**38**) and AV-45 (Amyvid, **39**) were selected.⁴² These candidates have more or less met the criteria used for developing compound **37**: (1) high binding affinity to A β aggregates ($K_i < 10$ nM); (2) high binding selectivity (K_i for other sites, >100-fold; of particular importance is that there is no tau binding); (3) easily labeled with ^{18}F for imaging with a radiochemical yield ranging from 20% to 35%; (4) a class of molecules with low MW (< 500), acceptable lipophilicity (measured $\log P = 0.1-3.5$), and neutral; (5) good initial brain uptake and desirable pharmacokinetics (high initial uptake of >6.0% dose/g at 2

min after iv injection and fast washout at 30 min, less than 30% of initial uptake remaining in the brain of normal mice); (6) high brain uptake and fast washout in primate brain by PET imaging.⁴¹



38



39

Initial clinical trials of **38** suggested that the brain uptake was lower than expected. This is due to a rapid *in vivo* metabolism via *N*-demethylation. The monodemethylation of **38** led to the formation of **39**, which exhibits excellent brain uptake and washout in humans. The signal-to-noise ratio in the brain reaches an optimal level in 40-60 min after iv injection. Therefore, PET imaging in AD patients is easier to perform.⁴¹

Amyvid (**39**), approved for A β imaging, is a PIB derivative that has a stilbene core, a styrylpyridine moiety and a polyethylene glycol (PEG) linker that.⁶⁷ The PEG linker can modulate lipophilicity and therefore allow the agent to more effectively cross the BBB and clear the brain readily and the styrylpyridine derivative reduces lipophilicity further.⁴¹⁻⁴⁴ The PEG group also keeps the compound at a relatively low molecular weight.⁴⁴ Amyvid also uses ¹⁸F as its radiolabel^{41,44}, allowing for a half-life of 110 minutes, which makes it more available for regional distribution clinical use.

Tau Hypothesis

The aforementioned weaknesses of the amyloid hypothesis might suggest that targeting amyloid β is not the correct route in diagnosing, curing, or even slowing down the progression of AD. Another theory to help diagnosis AD is the “tau hypothesis.”⁴⁷ The primary function of the microtubule-associated protein (MAP) tau protein is the stabilization of microtubules (MTs) that send nutrients to the neurons.⁴⁷ MAP tau is most abundant in the axons of neurons.⁴⁷ There are six major isoforms of tau expressed in the adult human brain, all of which are derived from a single gene by alternative splicing.⁴⁷ Tau is characterized by the presence of an MT-binding domain composed of repeats of a highly conserved tubulin binding motif⁴⁸ and which comprises the carboxy terminal (C-terminal) half of the protein, followed by a basic proline-rich region and an acidic amino-terminal (N-terminal) region, which is normally referred to as the ‘projection region’. The six tau isoforms differ from each other in the number of tubulin-binding repeats (either three or four, hence the isoforms are normally referred to as 3R and 4R tau isoforms, respectively) and in the presence of either one or two 29 amino-acids long inserts at the N-terminal portion of the protein, which is not instrumental for MT-binding.⁴⁹ Although the six isoforms appear to be broadly functionally similar, each is likely to have precise, and to some extent distinctive, physiological roles. The various isoforms appear to be differently expressed during development, however, the 3R and 4R tau isoforms are expressed in a one-to-one ratio in most regions of the adult brain, and deviations from this ratio are characteristic of neurodegenerative frontal temporal dementias (FTD) tauopathies.⁵⁰

In healthy neurons, tau normally has a certain amount of phosphate molecules attached and binds to microtubules and stabilizes them.⁴⁷ In AD and related

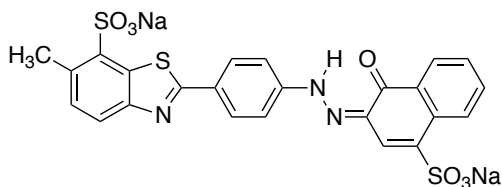
neurodegenerative disorders that are collectively referred to as tauopathies,^{51,52} tau becomes hyperphosphorylated and no longer binds to the MTs; instead it becomes sequestered into neurofibrillary tangles (NFTs) in neurons, and into glial tangles in astrocytes or oligodendroglia. In AD, the largest burden of tau pathology is found in neuronal processes known as neurophil threads or dystrophic neurites.⁵³ The pathological consequences of these events could result from a loss of normal tau function combined with gains of pathological functions of hyperphosphorylated tau, the filaments formed thereof, and the aggregation of these filaments to form glial and neuronal tangles in dystrophic neurites.⁴⁷

The loss of tau's normal MT-stabilizing function would invariably lead to a pathological disturbance in the normal structural and regulatory functions of the cytoskeleton, which would compromise axonal transport and thus contribute to synaptic dysfunction and neurodegeneration.^{54,55} The importance of the loss of the MT-stabilizing function of tau in neurodegeneration was recently validated by proof-of-concept studies carried out *in vivo*, which demonstrated that the MT-stabilizing drug paclitaxel can ameliorate the neurodegenerative phenotype of transgenic mouse models of AD-like tau amyloid pathologies.^{56,57} However, the discovery that the total level of NFTs correlates with the degree of cognitive impairment^{58,59} provide the initial circumstantial evidence to suggest that toxic gains-of-function by NFTs might play an important part in the progression of the disease.

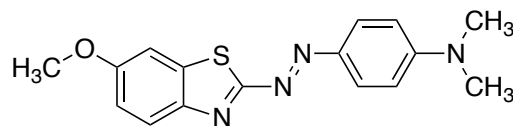
Small Molecules for Imaging Tau

In the pursuit of selective binding molecules for tau, small molecules were screened to differentiate between amyloid- β plaques, tau neurofibrillary tangles and α -synuclein.⁶⁰ To differentiate between these proteins, a library of 72,455 entities was screened to establish binding to the tau protein by observing changes in thioflavin-S (ThS) fluorescence, followed by a second screening to distinguish the affinity for each individual protein.⁶⁰ From this library of compounds, molecules demonstrating a >10-fold binding selectivity among these substrates were discovered, wherein those that were selective for tau aggregates were found to have at least three aromatic or rigid moieties connected by two rotatable bonds.⁶⁰ During the first screening, 72,455 compounds were screened with thioflavin-S (ThS) fluorescence to monitor tau conformation.⁶⁰ ThS-reactive tau was prepared with octadecyl sulfate (ODS), which is an alkyl sulfate inducer of tau conformational change and aggregation.⁶⁵ Full length tau was used as a substrate because it aggregates in early stages of AD, therefore representing an early marker of AD progression.⁶⁰ Of the molecules screened in the first stage, 45 compounds representing 35 active and 10 structurally related inactive analogs were chosen for a follow up study.⁶⁰ For the second screening, ODS was replaced with arachidonic acid to exclude nonspecific alkyl-sulfated mediated effects in ThS. Of the 35 active compounds identified in the first screening, all but eight showed similar dose response curves and half-maximal activity concentration (AC_{50}) values in the presence of arachidonic acid.⁶⁰ The eight compounds were then removed from study and compounds **40** (Thiazine red R) and **41** were added to the library because of their high affinity for binding to protein aggregates.⁶⁰ Thiazine red **40** selectively binds to neurofibrillary lesions in AD tissues while **41** binds to A β aggregates *in vitro*.^{61,62} The final test set contained 39 compounds,

of which 29 showed $AC_{50} < 10 \mu M$ (including nine with submicromolar AC_{50}) and 10 were inactive analogs.⁶⁰

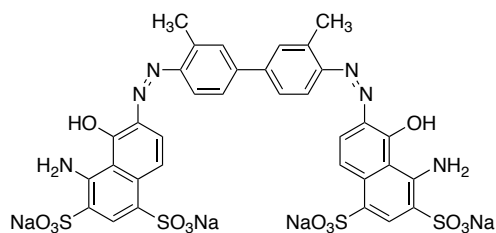


40

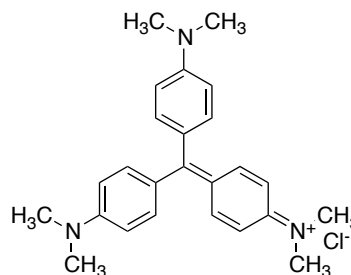


41

The active small molecules were placed into 6 scaffolds categories: benzothiazole, phenylazenes, quinoxaline nitriles, anilines, anthraquinones and indolinones.⁶⁰ These compounds were then measured for their relative affinity for tau, α -synuclein, and $A\beta_{1-42}$. Several of the compounds measured exhibited significant fold selectivity for tau relative to at least one other substrate.⁶⁰ Of these compounds, Evans blue (**42**) and aniline crystal violet (**43**) were exclusively selective for tau against both α -synuclein and $A\beta_{1-42}$. A third compound, Thiazine red (**40**) was the most selective ligand for tau, having a >17 fold selectivity for tau relative to α -synuclein and a >10 -fold selectivity to $A\beta_{1-42}$.⁶⁰

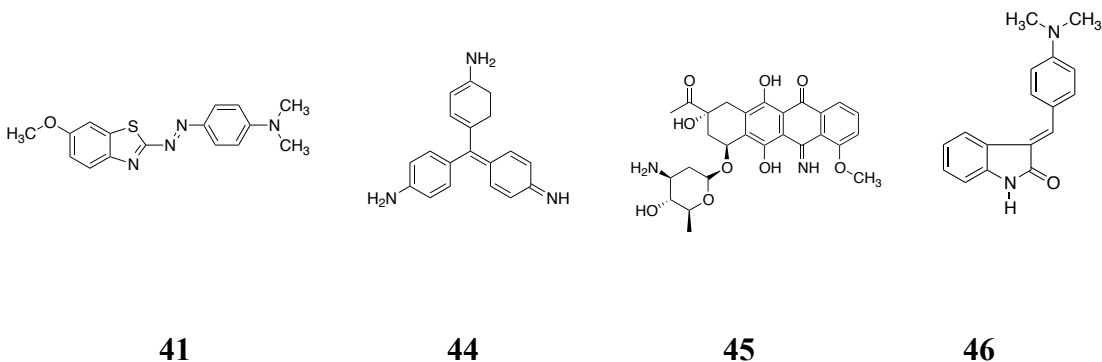


42



43

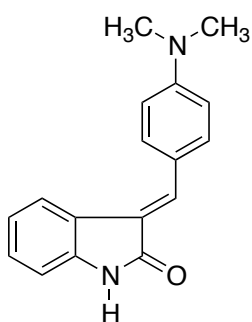
Benzothiazole **41**, the aniline **44**, the anthraquinone **45**, and the indolinone **46**, were all selective for both tau and A β ₁₋₄₂ relative to α -synuclein, with the benzothiazole being most potent with K_i of 7.8 nM.



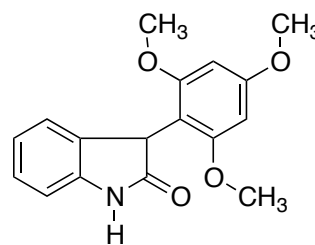
Evans blue (**42**) was less selective for tau than Thiazine red (**40**), but was 10-fold more potent in all assays, while crystal violet (**43**) was the most potent of all the substrates, however it showed only subtle selectivity.⁶⁰

Kuret et al.⁶⁰ found that aggregates composed of tau, α -synuclein, and A β ₁₋₄₂ display an overlapping variety of small molecule binding affinities. The six different scaffold classes that were studied showed tau aggregates to be the most discriminating substrate tested with the strongest binding affinities. The α -synuclein fibrils were the least discriminating and exhibited weaker overall affinity for the test compounds. Ligand selectivity and binding affinity of the compounds for A β ₁₋₄₂ aggregates were intermediate between those of tau and α -synuclein. The benzothiazine **40** and phenylazene **42** were exclusively selective for tau.⁶⁰ These two compounds shared structural features that include at least three aromatic or rigid moieties connected by two rotatable bonds.⁶⁰ This organization allows for the rings to be separated, which allows for certain geometries that may be beneficial for selectivity.⁶⁰ These structures are completely planar, a feature

which has also been proposed to be beneficial for tau binding.⁶³ Another common feature for tau binding is the presence of a hydroxyl group *ortho* to an azo linker like the one in **41**, which has been postulated to favor the hydrazone over the azo tautomer, thereby creating a six-membered ring through hydrogen bonding which would result in a third ring possibly being important for selective interactions with tau filaments. Benzylidene oxindole **47** was an effective binder of all filamentous substrates tested and antagonized tau fibrillation. Interestingly, the structurally similar indolinone **48** did not bind to any aggregates tested. This could be due to the fact that the 1,2,3-trimethoxy substituted aromatic ring is closer to the indolinone ring.⁶⁰



47

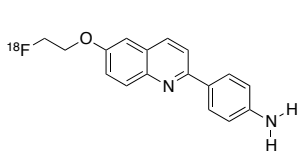


48

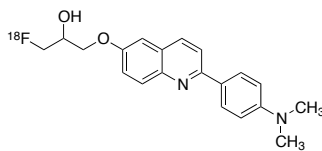
The goal of Kuret's work was to find a small molecule to serve as a vector for a possible tau-imaging agent for the diagnosis of AD.⁶⁴ Since β -amyloid may not be the best biomarker for AD diagnosis, another promising area could be tau neurofibrillary tangles. Like most good imaging agents, tau-imaging agents must fulfill four criteria to fulfill their diagnostic potential.⁶⁴ First, a good tau-imaging agent must be able to cross the BBB after intravenous injection while it rapidly leaves the brain. Second, the tau imaging agents should be capable of engaging their target within cells undergoing

neurofibrillary degeneration. Third, tau-directed radiotracers must bind a target that varies in composition and post-translation modification. Finally, successful radiotracers must bind tau aggregates with sufficient selectivity so that neuritic lesion spatial distribution is not masked or confounded by other lesions that appear in the disease.⁶⁴

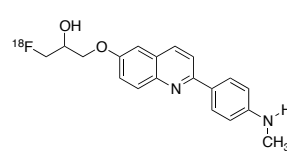
There has been previous progress in developing a tau-selective PET radioligand. One study is by a group at the Tohoku University/Austion Hospital in Melbourne, who synthesized a series of ¹⁸F-labeled aryl quinoline derivatives. The compounds that were best at binding to tau protein were compounds THK-523 (**49**), THK-5105 (**50**), and THK-5117 (**51**). *In vitro* binding assays demonstrated that **50** and **51** had a higher binding affinity for tau protein aggregates than **49**. Autoradiographic analysis of AD brain lesions of these compounds showed that these radiotracers preferentially bound to neurofibrillary tangles and neutrophil threads. These derivatives demonstrated ample initial brain uptake and faster clearance in normal mice compared to **49**. Compound **50** and **51** showed no toxic effects related to the administration of these compounds in mice and rats and no significant binding for various neuroreceptor, ion channels, and transporters.⁶⁸



49

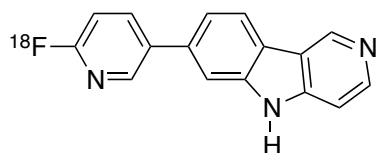


50

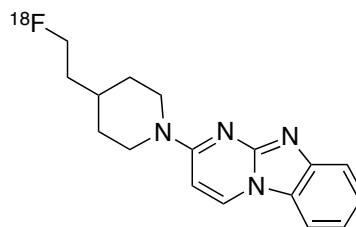


51

A Siemens/Lilly group reported the ^{18}F -labeled T807 (**52**) and T808 (**53**) compounds. Both groups have focused initially upon the binding of their tau-selective radioligands in the AD brain.



52



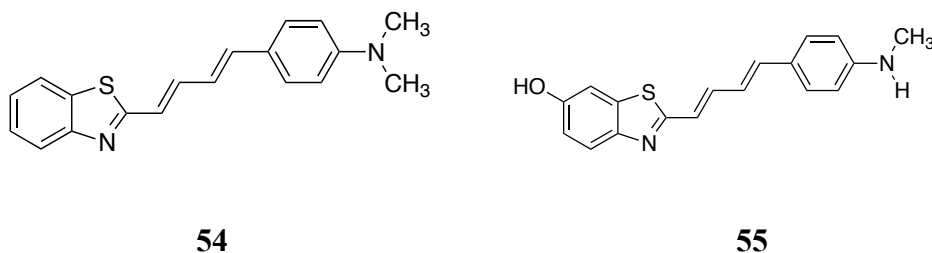
53

The Siemens/Lilly group found that in a study involving 6 human subjects, **52** showed a consistently higher standardized uptake value ratio (SUVR) in the AD subjects (1.20-1.80) compared to the MCI (1.02-1.38) and HC subjects (1.03-1.16) across the temporal lobe, parietal lobe, frontal lobe, and hippocampal area. The pattern of tracer retention overlaps with the known areas of paired helical filaments (PHF) tau formation according to Braak staging, strongly suggesting that **52** is a promising new biomarker for detecting tau deposits in AD patients.⁶⁹

Studies of radiotracer **53** in 11 subjects showed promising in vivo imaging of PHF-tau in AD subjects. The tracer displayed favorable distribution and uptake kinetics with a rapid delivery into the brain and clearance from non-target tissues. These results suggest the possibility of brain imaging as early as 30 min after injection. All subjects tested showed low tracer retention in the cerebellum and white matter. The HC subjects showed little radiotracer retention in the cortical gray matter. The activity in bone resulting from [^{18}F]-defluorination is separated from the cortical gray matter and does not

interfere with the imaging evaluation, especially at early time points. The more severely demented subjects generally showed higher tracer retention across more brain regions than less severely demented or HC subjects, suggestive of binding to PHF-tau deposits, with one exception being a 96-year-old dementia patient who did not show increased radiotracer retention.⁷⁰

Additionally, in terms of tau selective agents, Maruyama et al. studied the *in vitro* and *in vivo* properties of phenyl/pyridinyl- butadienyl-benzothiazoles/benzothiazoliums (PBB). Two, in particular, are compounds PBB1 (**54**) and PBB3 (**55**).^{71,72}



These PBB compounds fluoresce and are used in *in vitro* assays and *in vivo* optical imaging studies in transgenic tauopathy mouse models. Maruyama *et al* screened compounds **54** and **55** for selective binding to tau deposits (from both AD and non-AD tauopathies) over A β plaques with the most promising compound being PBB3 (**55**). Maruyama found that compounds with extended conjugated backbones of 13 to 15 Å bound most favorably to tau.⁷² The conjugated butadiene linkage between the two aromatic ring systems of PBBs provides the basis for their high tau binding affinities. The structural similarities between **12** and **55** are interesting to note because their binding affinities to aggregated A β and tau are very different. It is also important to note the difference in selectivity between **54** and **55**. Just like compound **12**, compound **54** also

binds to A β plaques.⁷¹ Possessing π -electron conjugated backbones; these compounds exhibit affinities for pathological inclusion in a broad range of tauopathies.^{71.72}

In vivo and *ex vivo* fluorescence imaging of tau inclusions with PBBs utilized PS19 transgenic mice expressing a FTDP-17 four-repeat tau isoform with the P301S mutation, and tau deposits were apparent in the brain stem and spinal cord of the mice. Other fluorescence imaging experiments were conducted in a second mouse model tauopathy (rTg4510 mice expressing the FTDP-17 four-repeat P301L mutation), and these mice demonstrated specific binding of PBBs to neuronal tau inclusions in the neocortex and hippocampus. In addition, several PBBs were radiolabeled with ¹¹C and examined in the mice after intravenous injection using *ex vivo* autoradiographic analysis and microPET imaging. In the event, [¹¹C]**55** performed well in the experiments and demonstrated low nonspecific binding, high specific binding to tau deposits, and saturable specific binding.⁷²

The binding of [¹¹C]**55** was also compared to [¹¹C]**12** using *in vitro* autoradiography of hippocampal sections of AD and control brains, and clear binding differences were observed. This comparison is consistent with specific binding of [¹¹C]**55** to tau deposits in NFTs and neurofibrillary threads and the absence of specific [¹¹C]**12** binding to these structures. PET imaging studies with [¹¹C]**55** were conducted in subjects with normal cognition, probable AD, or probable CBD and compared to those with [¹¹C]**12**. Compound [¹¹C]**55** showed lower nonspecific white matter binding than [¹¹C]**12** in all subjects, but probable AD subjects showed elevated retention with [¹¹C]**55** in medial temporal regions relative to [¹¹C]**12** as well as high levels of [¹¹C]**55** retention in

lateral temporal and frontal cortical areas relative to the control subjects. The *in vivo* behavior of [¹¹C]**55** in the brains of probable AD in control subjects was consistent with that of a tau-selective radiopharmaceutical and was distinctly different from the binding pattern of the A β -selective imaging agent [¹¹C]**12**. PET scans using [¹¹C]**12** and [¹¹C]**55** in the single CBD subject resulted in low levels of [¹¹C]**12** retention throughout the brain but significant retention of [¹¹C]PBB3 in neocortical and subcortical regions.⁷¹

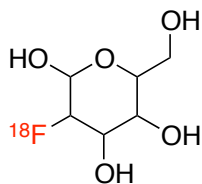
The pharmacokinetic properties of the radioligand **55** are generally favorable, with rapid brain uptake, relatively fast clearance of tracer from brain regions containing low tau loads, reversible specific binding of the tracer in tau-containing brain regions, and the absence of lipophilic radiolabeled metabolites in the blood. There are, however, several issues that remain for the use of **55** as a tracer: (1) the basis of the relatively high retention of the tracer in the dural venous sinuses of human subjects; (2) binding and imaging data in three-repeat predominant tau isoform cases such as Pick's disease; (3) the practical impact of the relatively low specific signal of [¹¹C]PBB3 in brain regions of high tau load (only 1.5 SUVR units) with respect to detection sensitivity limits in a variety of subjects; (4) thorough pharmacokinetic analyses of the radioligand in control, probable AD, and three- and four-repeat non-AD tauopathies; (5) critical comparison of the properties of [¹¹C]PBB3 relative to those of other putative tau-selective PET imaging agents such as the ¹⁸F-labeled THK compounds and the **52** and **53** and; validation of tau quantification in correlative imaging-postmortem studies as have been done for several A β -imaging tracers.^{71,72}

Consideration of Benzylidene Oxindoles as Potential Tau Binding Agents

As described earlier, benzylidene oxindoles represent one of six identified classes of molecules demonstrated to exhibit selective binding to the tau protein. Benzylidene oxindoles are nitrogen-linked Michael acceptors that are most commonly regarded as protein kinase inhibitors. Such compounds were amongst the first to be identified as receptor tyrosine kinase (RTK) inhibitors. SUGEN in 1998 found that: (1) 3-[(five-membered heteroaryl ring)methylidanyl]indolin-2-ones are highly specific against the vascular endothelial growth factor [VEGF (Flk-1)] RTK activity; (2) 3-(substituted benzylidenyl)indolin-2-ones containing bulky groups in the phenyl ring at the C-3 position of indolin-2-ones showed high selectivity toward the EGF and Her-2 RTKs and; (3) pyrrolic compounds containing an extended side chain at the C-3 position of indolin-2-one exhibit high potency and selectivity when tested against the PDGF and VEGF (Flk-1) RTKs.⁷³ Crystallographic data show that both the proton at the *N*-1 position and the oxygen at the C-2 position of indolin-2-ones bind to the peptide backbone with ATP binding pockets of these RTK, and it was reasoned that bidentate hydrogen bonding between the indolin-2-one flat core structure in the adenine binding site may play a crucial role to block entry of ATP in the binding site.⁷³ Both the proton at the *N*-1 position and the oxygen atom at the C-2 position of the indolin-2-one were found to be coordinated to the peptide backbone within the adenine-binding cleft. Additionally, alkylation at the *N*-1 position of the indolin-2-one greatly decreases the inhibitory potency of these 3-substituted indolin-2-ones against both the PDGF and VEGF (Flk-1) RTKs.⁷³ Thus, since the binding site of benzylidene oxindoles to tau protein is not known, it will be important to determine whether or not the *N*-H functionality, critical for kinase inhibition, is a necessary requirement for tau binding.

PET and SPECT Imaging

Since this thesis deals with the design and synthesis of medical imaging agents, it only remains to provide a brief overview of the technology involved. There are two types of nuclear medicine imaging devices: single photon emission computed tomography (SPECT) and positron emission tomography (PET). The radionuclides utilized play an important part for PET and SPECT imaging based on their physical characteristics of different half-lives and mode of decay.⁴¹ Mode of decay is the emitting of a single photon or in the case of PET a positron which is subsequently annihilated with a neighboring electron to emit two 511 keV photons at 180° apart.⁴¹ PET and SPECT have been reported for measuring changes in regional glucose metabolism and blood flow with aging and dementia.⁴¹ For instance, [¹⁸F]-2-fluoro-2-deoxyglucose (**56**, FDG) is a PET radiotracer that has been shown to improve the routine clinical diagnosis of suspected AD. When a patient presents clinical symptoms of dementia, cerebral rate of glucose (CMR_{glc}) reductions have occurred that are detectable on ¹⁸F-FDG PET scans as specific patterns of regional hypometabolism as compared with age-matched healthy elderly individuals.⁷⁴

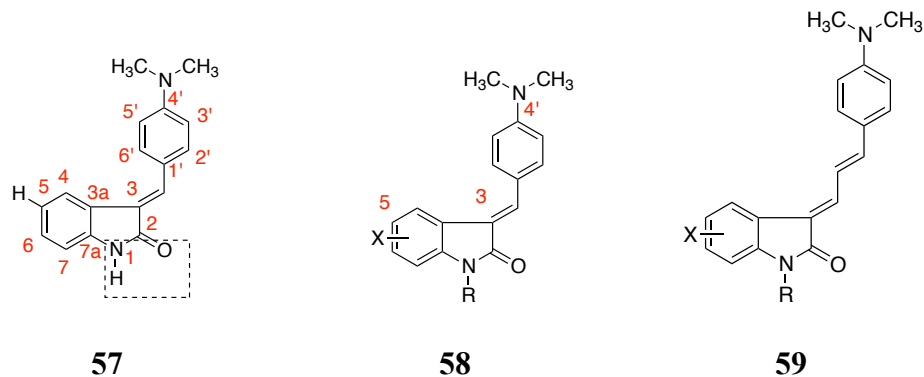


56

Results and Discussion

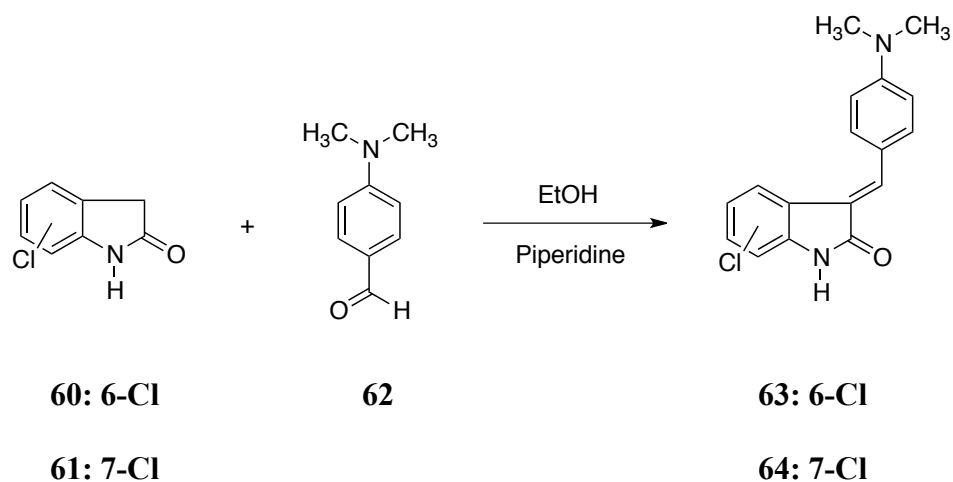
In light of the findings by the Kuret group that benzylidene oxindoles were one of six classes of organic molecules to display high affinity for the tau protein,^{60,64} the WSU group initiated a program of research to examine the utility of such molecules in the area of Alzheimer's disease (AD) as potential vectors for tau directed imaging agents. From the outset, SAR information was negligible since only two benzylidene oxindoles (based upon the kinase inhibitor SU4312 **57**) were examined. In this regard, the Kuret study indicated that substitution of an iodo substituent (versus -H) at the C-5 position of **57** had little effect on tau binding. This is rather unusual as there are substantial differences in the size and polarizability of these two substituents. Our overall plan, therefore, was to ascertain: a) if the nature and/or position of a halogen on the benzenoid ring affects tau binding; b) if substitution of such benzylidene oxindoles with *N*-alkyl groups inhibited tau binding, and; c) if extending the conjugation of the scaffold leads to an increase in tau/A β binding (*vide infra* compound **59**).

In the hopes that binding to tau might be modulated by appropriate substitution of the benzenoid ring of benzylidene oxindoles, we were rewarded by the fact that both chloro and fluoro substituents at C-5 were found to improve tau binding (*Kuret / Ketcha / Knisley unpublished results*). Moreover, since the 5-chloro substituent appeared to exhibit better binding than the 5-fluoro analogue, we next sought to examine the role of positional isomerism for chloro substituents.⁷⁹



To that end, both the 6- and 7-chloro-2-oxindole derivatives **60** and **61** were purchased from Sigma Aldrich (\$47.20/5g and \$53.40/1g respectively) and were allowed to react with 4-(dimethylamino)benzaldehyde (**62**) in ethanol and a catalytic amount of piperidine to afford the desired benzylidene oxindoles **63** and **64**.⁷³

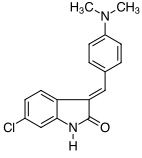
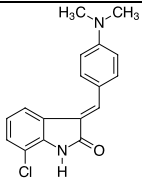
Scheme 1



Although the data is not provided herein, it was found by the Kuret group that the 6- and 7-chloro-3-(4-dimethylaminobenzylidene)indolin-2-ones, **63** and **64**, were less

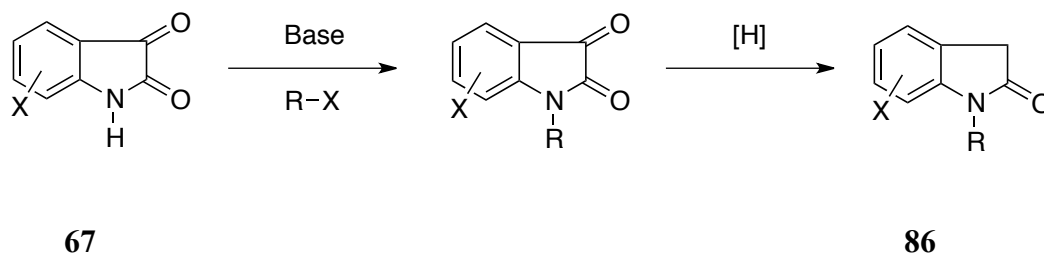
effective than the 5-Cl derivative in terms of tau binding. **Table 1** shows the respective compounds with their percent yields and melting points. As will be detailed later, the 6- and 7-chloro-3-(4-dimethylaminobenzylidene)indolin-2-ones were observed to exist as mixtures of the *Z* and *E* stereoisomers about the exocyclic double bond. The proportion of *E* or *Z* isomer is typically found to be dependent on the characteristics of the substituents placed at the C-3 position as well as the solvent employed for the NMR. Through the use of ¹H NMR analysis, the ratio of *E* or *Z* isomer could be determined due to the chemical shifts of the aromatic protons on the benzylidene ring (H-2' and H-6') at the C-3 position of the oxindole core (*vide infra*). In **Table 1**, the *Z* isomer is presented as a percentage along with the chemical shifts of the aromatic protons from the benzylidene (H-2' and H-6') proton NMR peaks. Since there was a mixture of the *E* and *Z* isomers, the values for the H-2' and H-6' proton NMR peaks (which appear as doublets, were used for both isomers if applicable) are provided.

Table 1: 3-Substitued Indoline-2-ones from Knoevenagel Condensation

	Compound	Percent yield	Melting point	Z%	<i>Z</i> isomer, H-2'-6' NMR shift, ppm	<i>E</i> isomer, H-2'-6' NMR shift, ppm
63		75%	253-256°C	30	8.44	7.76
64		89%	259-261°C	90	8.47	7.76

Having begun to explore the positional effects of chloro substituents on tau binding, we next sought to examine the role of an *N*-alkyl substituent. To that end, it was deemed necessary to develop a practical synthesis of *N*-methyl oxindoles to see if having a small alkyl group at the nitrogen position would affect tau binding. Since oxindoles display ambident reactivity at the nitrogen and the C-3 position in alkylation processes,^{75,76} it is common practice to *N*-alkylate the corresponding isatins in the presence of an appropriate base and then reductively deoxygenate the C-3 ketone carbonyl with a Wolf-Kishner type reaction to obtain the *N*-alkylated oxindole (**Scheme 2**).

Scheme 2



The Ketcha group had previously reported two methods for the expedient *N*-alkylation of isatins employing either KF/alumina in acetonitrile (ACN) or 1,8-diazabicyclo-[5.4.0]undec-7-ene (DBU) in ethanol.⁷⁷⁻⁸⁰ In these previous studies, alkylations were only conducted with benzylic halides derivatives and propargyl halides as alkylating agents. So it was therefore necessary to examine if a small alkyl group could be likewise be introduced at the nitrogen position, and if such molecules could readily be reduced to the corresponding -alkyl oxindole prior to the ultimate and aldol

condensation. Employing the former method, it was found that alkylation of isatin using iodomethane (1.5 eq) in the presence of KF/alumina⁸⁴⁻⁸⁵ afforded 1-methylindoline-2,3-dione (**65**) in moderate yields. It was also found that alkylation of isatin using iodomethane (1.5 eq) in DMF (5 mL) with K₂CO₃ (1.3 eq) as a base resulted in a purer product and involved an easier workup, when compared to using KF/alumina. **Table 2** shows the respective conditions employed. yields and melting points of 1-methylindoline-2,3-dione (**65**)

Scheme 3

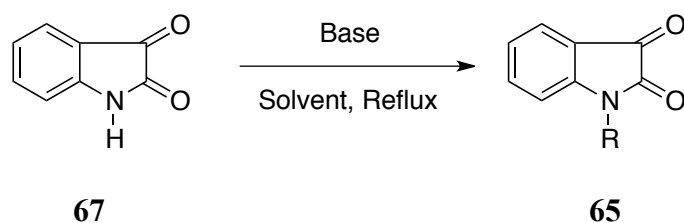
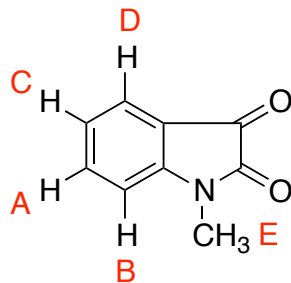


Table 1: 1-Methylindoline-2,3-dione

	Compound	Base	Percent Yield	M.P	Lit. M.P
65		K ₂ CO ₃ /DMF ⁸¹	51%	129-131°C	130-133°C ⁸¹
		KF/Al ₂ O ₃ /ACN ⁸⁴	60%	119-120°C	



65

A proton NMR spectrum (**Figure 1**) for compound **65** shows that there is a triplet of doublets furthest downfield at 7.59 (H_A , $J = 1.13$ Hz, $J = 7.79$ Hz), a doublet at 7.54 (H_B , $J = 7.47$ Hz), a triplet at 7.10 (H_C , $J = 7.53$ Hz), a doublet at 6.89 (H_D , $J = 7.91$ Hz) and a singlet at 3.22 ppm (H_E). These data correspond to NMR data from Sigma-Aldrich's website.⁹¹ (**Figure 2**).

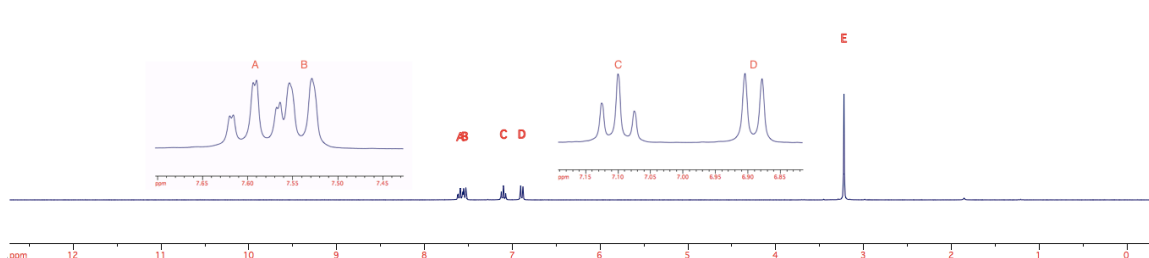


Figure 1: ^1H Proton of 1-methylindolin-2,3-one

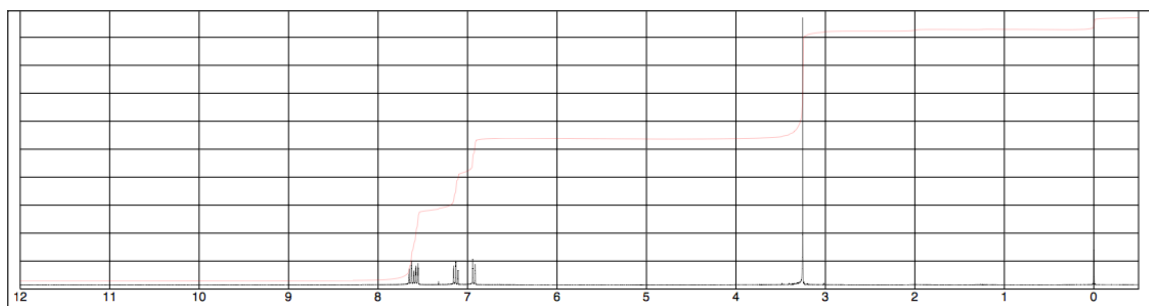
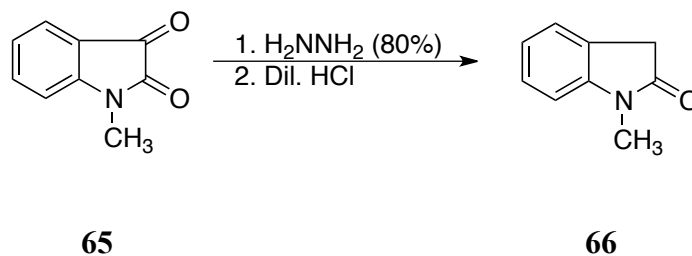


Figure 2: ^1H Proton of 1-methylindolin-2,3-one

Having in hand the requisite *N*-methylisatin, it was then necessary to establish if this compound could then be reduced under Wolf-Kishner conditions to the corresponding oxindole⁸⁶ in anticipation of condensation with a variety of benzaldehydes possessing various electron-donating groups to afford a small library of *N*-methylbenzylidene oxindoles for tau binding studies. The traditional route employed in this research group was to treat the isatin (1 mmol) with hydrazine hydrate 80% (15 mL) for 3 h with moderate heat and then acidify the solution with 3M HCl to a pH of 4 and let the resulting solution sit overnight.⁸⁰ In this case, this traditional route seemed ineffective because the product, upon standing, failed to fall out of solution. The reaction was tried again, but rather than waiting overnight for crystallization to occur, the reaction mixture was extracted with ethyl acetate (3 x 30 mL) and evaporated under reduced pressure to yield a brown oil. The oil was then recrystallized from dichloromethane/hexanes to afford a white solid in very low yields (e.g., 60%) to afford 1-methyl-2-oxindole (**66**). However, although the observed melting point (70-73°C) was significantly lower than the literature value of 85-87°C, the compound was shown to be pure by GC/MS, TLC and NMR. Due to the observed low yield, it was brought to mind that 1-methyl-2-oxindole was available from Sigma-Aldrich at a modest cost of \$96.00/5g.

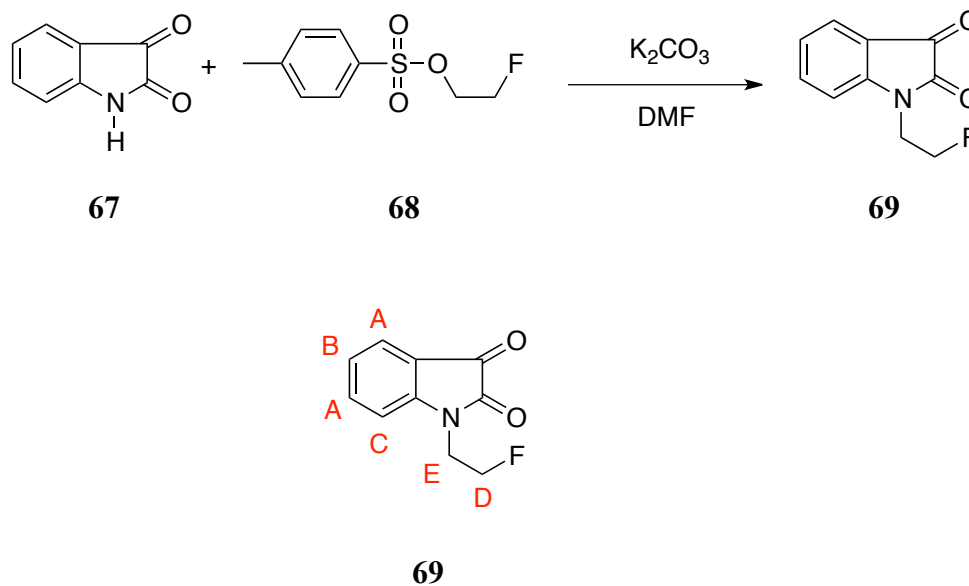
Scheme 4



In results not described herein, it was found that that *N*-methylation of benzylidene oxindoles does not negatively impact tau binding (Cox/Ketcha/Kuret unpublished). Having now a point of attachment for a possible radiolabeled fluorine reporter group we then sought to investigate similar benzylidene oxindoles bearing an *N*-2-fluoroethyl group as the cold version of a possible tau-imaging agent. The cold version is the non-radioactive version of the imaging agent, which would be used to see examine tau binding. If such “cold” versions exhibited the desired binding affinities, a radioactive fluorine could then be incorporated for PET imaging studies.

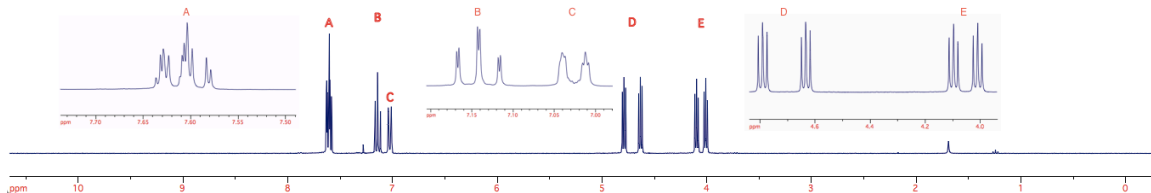
To that end, isatin (**67**) was *N*-alkylated with 2-fluoroethyl-tosylate (**68**) to produce the corresponding 1-(2-fluoroethyl)indol-2,3-dione (**69**) in 40 % yield with a melting point of 126-128°C (Scheme 5).

Scheme 5



A proton NMR spectrum (**Figure 3**) for compound **69** shows that there is a 2H multiplet furthest downfield at 7.64-7.58 ppm (H_A), a triplet of doublets at 7.14 (H_B , $J = 0.83, 7.55$ Hz, 1H), a 1H multiplet at 7.04-7.01 ppm (H_C), a doublet of triplets at 4.71 (H_D , $J = 4.76, 47.02$ Hz, 2H) and a doublet of triplets at 4.05 (H_E , $J = 4.76, 26.27$ Hz, 2H). The extra splitting at 4.71 and 4.05 ppm is due to the effects of the fluorine coupling with the hydrogens and has a coupling constant of 198 ppm.

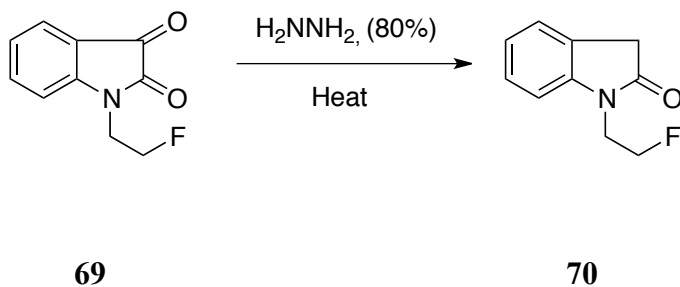
Figure 3: ^1H Proton NMR of 1-(2-Fluoroethyl)indol-2,3-one



The product **69**, was then reduced to the corresponding 1-(2-fluoroethyl)indol-2-one (**70**) in 60.7 % yield using hydrazine hydrate (80%) and refluxed for 2 h in a RBF wrapped with aluminum foil in an oil bath at 130°C. After 2 h, the solution was diluted with water (5 mL) and then extracted with ethyl acetate (3 x 30 mL), washed with brine (30 mL), dried (Na_2SO_4) and evaporated to afford brown solid (**Scheme 6**).

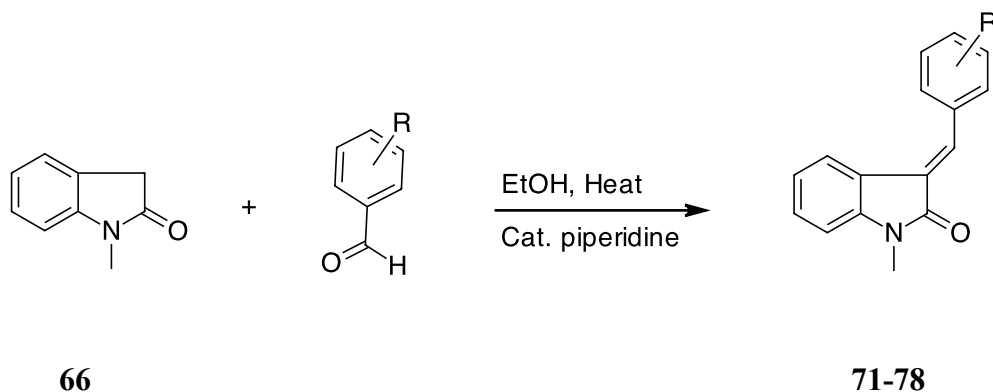
Having developed a synthesis of this fluoroethylated precursor, it now remains to conduct Knoevenagel condensations of **70** with various aromatic aldehydes bearing electron-donating groups to yield the “cold” versions of potential tau imaging agents

Scheme 6



Returning now to the case of the *N*-methyl oxindole analogs, Knoevenagel condensations with various aldehydes (1.2 eq) utilizing piperidine (0.147 eq) as a catalyst in ethanol (4 mL) were conducted to synthesize the desired library of *N*-methyl-3-substituted benzylidene oxindoles for tau binding studies. Since it appears as though *N*-alkylation (with substituents of modest size) does not inhibit tau binding properties, such a library might complement the analogous *N*-H versions in providing molecules with expectedly greater lipophilicity so as to allow for a range of BBB transport properties.

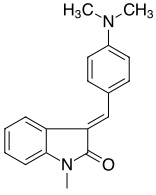
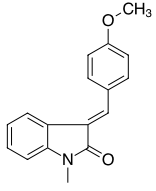
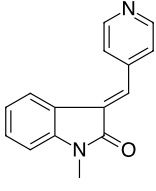
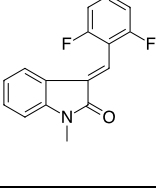
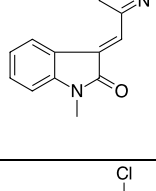
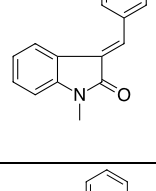
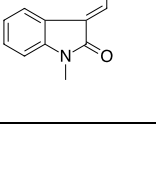
Scheme 7



The 3-substituted *N*-methylbenzylidene oxindoles thus prepared consisted of either the *E* or *Z* isomer or a mixture of the two. To determine the *E* or *Z* stereochemistry of the products, ¹H NMR analysis was used, wherein the *E/Z* isomer ratio could be determined by examination of the chemical shifts of the H-2' and H-6' aromatic protons on the benzylidene ring, and/or the fact that the vinylic proton can also be significantly influenced by configuration. If the compound were an *E* isomer, the vinylic proton (H_{vin}) is more deshielded due to the influence of the C-2 carbonyl just as their *ortho*-benzylidene (H_o) are shifted downfield due to the C-2 carbonyl. Therefore, in an *E* isomer, the H-2',6' protons would fall in the range of 7.45-7.84 ppm, compared to a *Z* isomer, in which the 2,6' protons would fall in the range of 7.85-8.53 ppm.⁸⁹ In cases where the 2',6' protons are substituted, only the influence of the vinylic proton was used to determine configuration, where the vinylic proton occurs about 7.84 ppm for *E* and 7.55 ppm for *Z*.⁹⁰ **Table 3** shows the *N*-methylbenzylidene oxindoles prepared and their properties. The chemical shifts are reported for the 2,6' protons unless they are substituted. In this case the chemical shift is report with the (H_{vin}). The areas of the two-isomer protons (H-2' and H-6') peaks were employed to calculate the percent *Z*. If the H-2' and H-6' were substituted then the vinylic protons are used to calculate the percent *Z*.

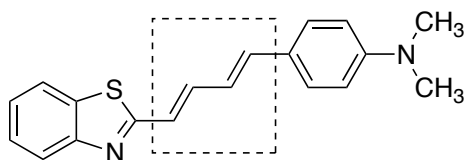
Table 3: *N*-Methyl benzylidene oxindoles

	Compound	Percent yield	Melting point	Z%	H-2' and H-6' proton δ (ppm) (Z)	H-2' and H-6' proton δ (ppm) (E)

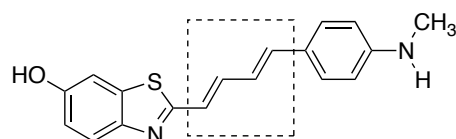
71		51%	156-159°C	100	8.49	N/A
72		41%	76-90°C	38	8.50	7.71
73		53%	77-81°C	48	8.72	7.61
74		29%	108-110°C	100	N/A	7.43 (Hvin)
75		72%	148-151°C	100	N/A	7.64 (Hvin)
76		23%	101-103°C	22	8.39	7.71
77		69%	168-171°C	100	N/A	7.64 (Hvin)

78		53%	209-212°C	0	N/A	7.79 (Hvin)
----	---	-----	-----------	---	-----	----------------

While the effects of a small *N*-alkyl group on the tau binding properties of benzylidene oxindoles were being evaluated, a paper came out which indicated that extended conjugated systems of 15-18 Å were in fact optimal for binding to tau protein (e.g., compounds **54** and **55** as discussed previously),.



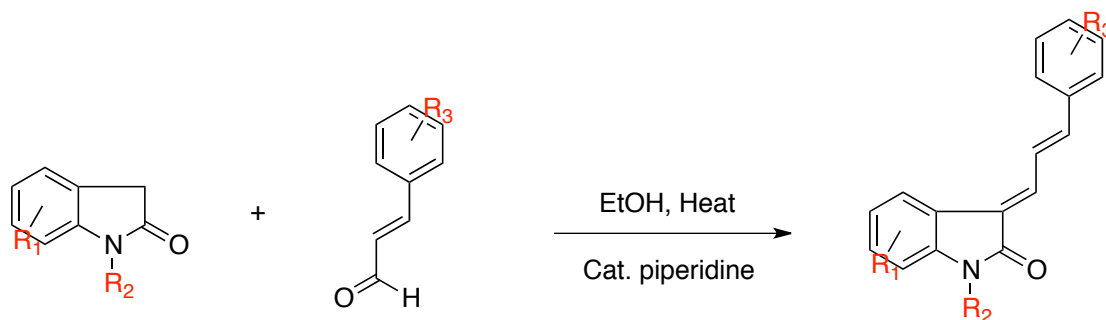
54



55

Accordingly, knowing that extended conjugated backbones enhance tau-binding properties, a new class of extended benzylidene oxindoles was synthesized with conjugated aryl aldehydes.

Scheme 8



66: $R_1 = H$; $R_2 = CH_3$

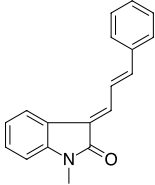
80-85

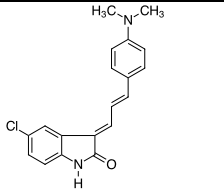
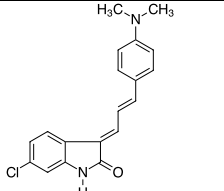
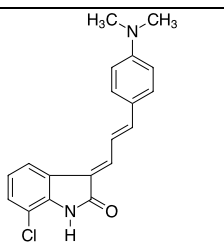
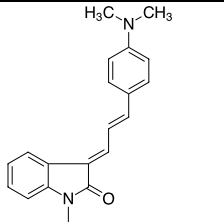
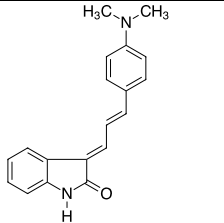
79: $R_1 = 5\text{-Cl}$; $R_2 = H$

To that end, *trans*-cinnamaldehyde (1.2 eq) was first reacted with 1-methyl-2-oxindole with piperidine as a catalyst (0.147 eq) to afford a red-brown solid, which was recrystallized with ethanol to yield 1-methyl-3-(3-phenylallylidene)indolin-2-one (**80**). In a similar manner, 5-, 6-, and 7-chlorooxindole were reacted with 4-(dimethylamino)cinnamaldehyde so as to provide extended versions of the tau binding parent possessing the dimethylamino substituted aryl ring compounds known to exhibit tau binding. The 5-chloro derivative in this case was obtained as a red solid, which was hard to purify because it was not very soluble in the solvents tested (DCM, MeOH, EtOH, benzene). It took an excessive amount of ethanol to recrystallize the product, which yielded relatively pure 5-chloro-3-(4-dimethylamino)phenylallylidene)indolin-2-one (**81**). The 6-chloro derivative was produced as a dark red solid, and it also took an excessive amount of ethanol to get the product back into solution to yield 6-chloro-3-(4-dimethylamino)phenylallylidene)indolin-2-one (**82**). Finally, the 7-chloro derivative was

produced as a dark purple solid and was insoluble in a number of solvents (DCM, MeOH, EtOH, benzene). In order to further purify this samples, whatever sample that did dissolve in ethanol was run through a silica gel column (70:30, hexanes:EtOAc) to yield 7-chloro-3-(4-dimethylamino)phenylallylidene)indolin-2-one (**83**). Interestingly, the reaction between 1-methyl-2-oxindole and 4-(dimethylamino)cinnamaldehyde produced a dark red oil, which could be easily dissolved in DCM and run through a silica gel column (70:30, hexanes:EtOAc) to produce 1-methyl-3-(4-dimethylamino)phenyl-allylidene)indolin-2-one as a red solid (**84**). Lastly, the reaction between oxindole and 4-(dimethylamino)cinnamaldehyde produced 3-(4-dimethylamino)phenylallylidene)-indolin-2-one as a red solid (**85**), which could easily be recrystallized with ethanol. **Table 4** shows the resulting compounds and their percent yields. The *E* and *Z* isomers were not calculated; because it was believe that significant isomerization was happening with the products when heated.

Table 4: 3-Substitued-indolin-2-ones from Knoevenagel Condensation

	Compound	Percent Yield	Melting Point
80		31%	162-164°C

81		47%	280-283°C
82		12.5%	269-271°C
83		74%	243-245°C
84		37%	159-161°C
85		13%	230-234°C

Summary

The purpose of this research was to design and synthesis a series compounds compounds that could one day be used as the next imaging agent for tau. It had previously been shown in our research group that a 5-chloro substituent on the indolinone ring displayed better binding to tau than a 5-fluoro substituent. It was therefore necessary

to establish the positional selectivity of such a chloro substituent, and to that end, the C-6 and C-7 chloro derivatives of 3-(4-dimethylaminobenzylidene)indolin-2-one were prepared. It was found that benzylidene oxindoles with a chlorine atom on the C-5 carbon was better in binding to tau than a chlorine atom on the C-6 and C-7 carbon of benzylidene oxindoles. Next, it was important to know whether a small alkyl group on the nitrogen of the indolinone would affect tau binding in any way. Having established (*Cox unreported*) that *N*-alkyl groups do not negatively impact tau binding, a library of 1-methyl-2-benzylidene oxindoles was synthesized. Finally, based on a recent disclosure that heterocycles with extended tethering to an aromatic ring with an electron-donating group (extended conjugated backbone of 15-18 Å) exhibited selective binding for the tau protein, a library of such compounds in which an aromatic ring bearing an electron donating was tethered to an indolinone ring was prepared.

The significant findings from this research as regards tau binding include: a) 5-chloro indolinones enhance tau binding relative to other positional isomers; b) relatively small *N*-alkyl substituents on the indolinone core do not inhibit tau binding and might be employed as a means of attaching an ¹⁸F-radiotracer for tau directed PET imaging agents, and; c) indolinones with extended conjugation are effective tau binding agents, and perhaps can be utilized as vectors for potential PET imaging agents.

Experimental

Chemical Analysis

Melting points were determined via the use of open capillaries with an Electrothermal melting point apparatus and are reported uncorrected. Elemental analyses were performed by Midwest Microlab, Indianapolis, IN. Elemental analysis results are within +0.4% of the theoretical values. The ^1H and ^{13}C NMR data were obtained on a Bruker Avance 300 MHz NMR in CDCl_3 or DMSO-d_6 solution unless otherwise indicated. The chemical shifts are reported in δ (ppm) downfield from tetramethylsilane as an internal standard; coupling constants (J) are in Hz. The following abbreviations are used to describe peak patterns where appropriate: s, singlet; d, doublet; dd, double doublet; t, triplet; q, quartet; dt, double triplet; m, multiplet. GC/MS measures were performed using an Hewlett-Packard 6890 Series GC and Agilent Technologies 7820A Series GC with auto injection and mass fragments are reported in, m/z . The GC's were coupled with a mass spectrometer with a Hewlett-Packard 5973 mass selective/quadrupole system and a Agilent Technologies 5975 mass selective/quadrupole system respectfully. Flash column (Silica Gel, Premium Rf, 200-400 mesh, Sorbent Technologies) and thin layer chromatography (TLC) were performed on silica gel with indicated solvents.

6-Chloro-3-(4-dimethylaminobenzylidene)indolin-2-one (63) (KWC-II-78)

To a 4 dram vial was added 6-chloro-2-oxindole (**60**) (0.2036 g, 1.215 mmol), 4-(dimethylamino)benzaldehyde (0.2280 g, 1.528 mmol, 1.2 equiv), piperidine (18 μL ,

0.179 mmol, 0.147 equiv) and EtOH (4 mL). The vial was heated at 90°C for 3 h while stirring. The mixture was allowed to cool to rt and placed in the freezer overnight, after which time a brown precipitate (0.2712 g, 75%) was collected by vacuum filtration and washed with EtOH: mp 253-256°C; LC/MS (*m/z*) 299 ($M^+ + 1$); $R_f = 0.61$ (1:1 Hexanes/EtOAc); $^1\text{H NMR}$ (300 MHz, DMSO- d_6) δ : 10.65 (bs, 1H, N-H), 7.76 (d, $J = 8.27$, 1H), 7.67-7.61 (m, 2H), 7.55 (s, 1H, H-Vinyl), 6.99-6.91 (m, 1H), 6.88-6.87 (m, 1H, H-7), 6.83-7.74 (m, 2H), 3.03 (s, 6H, $\text{N}(\text{CH}_3)_2$); $^{13}\text{C NMR}$ (75 MHz, DMSO- d_6) δ : 169.8, 1512.0, 143.8, 138.7, 132.9, 132.6, 123.2, 121.3, 121.2, 121.2, 120.9, 112.0, 110.1, 40.1. Anal. Calcd for $\text{C}_{17}\text{H}_{17}\text{ClN}_2\text{O}$: C, 68.34; H, 5.06; N, 9.38; Found: C, 68.18; H, 4.95; N, 9.34.

7-Chloro-3-(4-dimethylaminobenzylidene)indolin-2-one (64) (KWC-II-79)

To a 4 dram vial was added 7-chloro-2-oxindole (**61**) (0.2308 g, 1.377 mmol), 4-(dimethylamino)benzaldehyde (0.2535 g, 1.699 mmol, 1.2 equiv), piperidine (20 μL , 0.202 mmol, 0.147 equiv) and EtOH (4 mL). The vial was heated at 90°C for 3 h while stirring. The mixture was allowed to cool to rt and placed in the freezer overnight, after which time an orange precipitate (0.3658 g, 89%) was collected by vacuum filtration and washed with EtOH: mp 259-261°C; LC/MS (*m/z*) 299 ($M^+ + 1$); $R_f = 0.59$ (1:1 Hexanes/EtOAc); $^1\text{H NMR}$ (300 MHz, DMSO- d_6) δ : 10.88 (bs, 1H), 8.46 (d, $J = 9.01$ 2H), 7.72 (s, 1H, H-Vinyl), 7.60 (d, $J = 7.37$ Hz, 1H), 7.16 (d, $J = 8.03$, 1H), 6.96 (t, $J = 7.83$ Hz, 1H), 6.78 (d, $J = 9.03$, 2H), 3.05 (m, 6H, $\text{N}(\text{CH}_3)_2$); $^{13}\text{C NMR}$ (75 MHz, DMSO- d_6) δ : 168.0, 152.6, 140.5, 137.0, 135.6, 128.5, 126.7, 122.2, 122.1, 119.7, 117.3, 113.7,

111.5, 40.0 ppm. Anal. Calcd for C₁₇H₁₇ClN₂O: C, 68.34; H, 5.06; N, 9.38; Found: C, 68.30; H, 5.06; N, 9.31.

1-Methylindolin-2,3-dione (65): Route A

To a 250 mL RBF was added isatin (**67**) (1.2099 g, 8.223 mmol), KF/alumina (7.5675 g, 49.495 mmol, 6 equiv), iodomethane (767 μ L, 12.3 mmol, 1.5 equiv) and acetonitrile (45 mL). The resulting solution was refluxed overnight while stirring. After the mixture was allowed to cool to rt, the suspended KF/alumina was removed by vacuum filtration. The filtrate was then evaporated *in vacuo* and the resulting solid was recrystallized with DCM/hexanes to afford an orange solid (0.7988 g, 60.3%): mp 119-120°C (lit.⁸¹ mp 130-133°C); GC/MS (*m/z*) 161 (M⁺), 28 (100%); LC/MS (*m/z*) 162 (M⁺+1); R_f = 0.56 (1:1 Hexanes/EtOAc).

1-Methylindolin-2,3-dione (65): Route B (65) (KWC-II-63)

To a 4 dram vial was added isatin (**67**) (1.0306 g, 7.005 mmol), K₂CO₃ (1.2929 g, 9.355 mmol, 1.3 equiv), iodomethane (480 μ L, 7.705 mmol, 1.5 equiv) and DMF (5 mL). The vial was heated at 80°C for 3 h while stirring. The mixture was allowed to cool to rt and was then pour over ice to afford an orange solid (0.7162 g, 63.4%) and was recrystallized with EtOH (0.5718 g, 50.7%): mp 129-131°C (lit.⁸¹ mp 130-133°C); GC/MS (*m/z*) 161 (M⁺), 28 (100%); R_f = 0.56 (1:1 Hexanes/EtOAc). ¹H NMR (300 MHz, DMSO-*d*₆) δ : 7.59 (td, *J* = 1.13, 7.79 Hz, 1H), 7.54 (d, *J* = 7.47, 1H), 7.10 (t, *J* = 7.53 Hz, 1H), 6.89 (d, *J* = 7.91 Hz, 1H), 3.22 (s, 3H); ¹³C NMR (75 MHz, DMSO-*d*₆) δ : 183.3, 158.2, 151.4,

138.5, 125.1, 123.8, 117.4, 110.0, 26.2 ppm. Anal. Calcd for C₉H₇NO₂: C, 67.07; H, 4.38; N, 8.69; Found: C, 67.15; H, 4.37; N 8.71.

1-Methyl-2-oxindole (66) (KWC-I-64)

To a 250 mL RBF was added 1-methylindolin-2,3-one (**65**) (0.2531 g, 1.572 mmol) and hydrazine hydrate (80%, 15 mL). The RBF was then wrapped in aluminum foil and refluxed for 4 h. The solution was then acidified to a pH of 4 with dilute HCl (3M, 80 mL). No precipitate formed overnight so the solution was extracted with ethyl acetate (3x30 mL) and the combined organic layers were evaporated *in vacuo* to afford brown oil. The oil was then recrystallized with DCM/hexanes to afford a white solid (0.1395 g, 60.3%): mp 70-73°C (lit.⁸⁷ mp 85-88°C); GC/MS (*m/z*) 147 (M⁺), 28 (100%); R_f = 0.71 (1:1 Hexanes/EtOAc). ¹H NMR (300 MHz, DMSO-*d*₆) δ: 7.28-7.22 (m, 2H), 6.99 (td, *J* = 0.98, 7.47, 1H), 6.93 (d, *J* = 7.70 Hz, 1H), 3.49 (s, 2H), 3.09 (s, 3H): ¹³C NMR (75 MHz, DMSO-*d*₆) δ: 174.8, 145.4, 128.0, 125.1, 124.5, 122.2, 108.6, 35.5, 26.2 ppm. Anal. Calcd for C₉H₉NO: C, 73.45; H, 6.16; N, 9.52; Found: C, 72.99; H, 5.90; N, 9.33.

1-(2-Fluoroethyl)-indol-2,3-one (69) (KWC-II-68)

To a 4 dram vial was added isatin (**67**) (1.1937 g, 8.113 mmol), 2-fluoroethyl-tosylate (1.9625 g, 8.992 mmol, 1.2 equiv), potassium carbonate (1.4620, 10.58 mmol, 1.3 equiv) and DMF (4 mL). The vial was heated at 80°C for overnight while stirring. The mixture was allowed to cool to rt and pour into ice water, after which time a red precipitate (0.9261 g, 59.1%) was collected by vacuum filtration and recrystallized with EtOH (0.6312 g, 40.3%): mp 126-128°C; GC/MS (*m/z*) 193 (M⁺), 132 (100%); R_f = 0.57 (1:1

Hexanes/EtOAc); ^1H NMR (300 MHz, CDCl_3) δ : 7.64-7.58 (m, 2H), 7.14 (td, $J = 0.83$, 7.55 Hz, 1H), 7.04-7.01 (m, 1H), 4.71 (dt, $J = 4.76$, 47.02 Hz, 2H), 4.05 (td, $J = 4.76$, 26.27 Hz, 2H); ^{13}C NMR (75 MHz, CDCl_3) δ : 182.8, 158.4, 151.0, 138.5, 125.3, 123.9, 117.5, 110.8-110.7, 82.8, 80.5, 41.0, 40.7 ppm. Anal. Calcd for $\text{C}_{10}\text{H}_8\text{FNO}_2$: C, 62.18; H, 4.17; N, 7.25; Found: C, 61.99; H, 4.09; N, 7.32.

1-(2-Fluoroethyl)indolin-2-one (70) (KWC-II-75)

In a 5 mL RBF was added 1-(2-fluoroethyl)indol-2,3-one (**69**) (0.2180 g, 1.129 mmol) and hydrazine hydrate (80%, 720 μL). RBF was then wrapped in aluminum foil and refluxed for 2 hrs. Solution was then diluted with cold water (5 mL), extracted with EtOAc (3x30 mL), washed with brine (30 mL), and dried with Na_2SO_4 for 1 hr. The solution was then evaporated *in vacuo* to afford a brown solid. (0.1896 g, 93.8 %): mp 120-123°C; GC/MS (m/z) 179 (M^+), 118 (100%); $R_f = 0.42$ (1:1 Hexanes/EtOAc). ^1H NMR (300 MHz, CDCl_3) δ : 7.31-7.25 (m, 2H), 7.06 (td, $J = 0.93$, 7.51 Hz, 1H), 6.94 (d, $J = 7.87$ 1H), 4.68 (dt, $J = 4.98$, 47.08 Hz, 2H), 4.04 (td, $J = 4.98$, 25.59 Hz, 2H), 3.57 (s, 2H). Anal. Calcd for $\text{C}_{10}\text{H}_{10}\text{FNO}$: C, 67.03; H, 5.62; N, 7.82; Found: C, 65.94; H, 5.63; N, 8.17.

3-(4-Dimethylaminobenzylidene)-1-methyl-1,3-dihydro-indol-2-one (71) (KWC-I-82)

To a 4 dram vial was added 1-methyl-2-oxindole (**66**) (0.3983 g, 2.71 mmol), 4-(dimethylamino)benzaldehyde (0.3983 g, 3.25 mmol, 1.2 equiv), piperidine (39.2 μL , 0.398 mmol, 0.147 equiv) and EtOH (4 mL). The vial was heated at 90°C for 6 h while stirring. The mixture was allowed to cool to rt and placed in the freezer overnight, after which time a red precipitate (0.5845 g, 63.4%) was collected by vacuum filtration and

washed with EtOH to yield (0.3845 g, 51.04%): mp 145-155°C; GC/MS (m/z) 293 (M^+ , 100%); R_f = 0.75 (1:1 Hexanes/EtOAc); ^1H NMR (300 MHz, $\text{DMSO-}d_6$) δ : 8.47 (d, J = 9.24 Hz, 2H, H-2',6'), 7.68 (s, 1H, H-vinyl), 7.65 (s, 1H, H-4), 7.21 (dt, J = 1.10, 7.65 Hz, 1H, H-6), 7.01 (dt, J = 0.99, 7.53 Hz, 1H, H-5), 6.94 (d, J = 7.66 Hz, H-3',5'), 3.22 (s, 3H, N- CH_3), 3.03 (s, 6H, $\text{N}(\text{CH}_3)_3$ -4); ^{13}C NMR (75 MHz, $\text{DMSO-}d_6$) δ : 165.7, 151.8, 140.6, 138.2, 134.8, 132.0, 126.9, 124.9, 121.9, 121.0, 118.9, 118.0, 111.0, 107.8, 25.7 ppm. Anal. Calcd for $\text{C}_{18}\text{H}_{18}\text{N}_2\text{O}$: C, 77.67; H, 6.52; N, 10.06; Found: C, 77.52; H, 6.56; N, 10.23.

3-(4-Methoxybenzylidene)-1-methyl-1,3-dihydro-indol-2-one (72) (KWC-I-83)

To a 4 dram vial was added 1-methyl-2-oxindole (**66**) (0.2025 g, 1.38 mmol), *p*-anisaldehyde (200.9 μL , 1.65 mmol, 1.2 equiv), piperidine (20 μL , 0.202 mmol, 0.147 equiv) and EtOH (4 mL). The vial was heated at 90°C for 6 h while stirring. The mixture was allowed to cool to rt and was then placed in the freezer overnight. No precipitate formed so the solution was evaporated under reduced pressure to afford a red oil which was subjected to column chromatography (70:30 Hexanes:EtOAc) to afford a yellow oil which was recrystallized with DCM/hexanes to afford a yellow solid (0.1489 g, 40.6%): mp 65-70°C; GC/MS (m/z) 265 (M^+ , 100%); R_f = 0.75, 0.89 (1:1 Hexanes/EtOAc); ^1H NMR (300 MHz, $\text{DMSO-}d_6$) δ : 8.49 (d, J = 8.87 Hz, 1H), 7.68 (s, 1H, H-vinyl), 7.69 (t, J = 8.38 Hz, 3H), 7.33-7.24 (m, 1H), 7.11-6.91 (m, 4H), 3.84 (s, 3H, OCH_3 -4), 3.20 (s, 3H, N- CH_3); ^{13}C NMR (75 MHz $\text{DMSO-}d_6$) δ : 167.4, 165.4, 161.2, 160.6, 143.7, 141.4, 137.0, 136.5, 134.4, 131.5, 129.6, 128.1, 126.8, 126.4, 124.5, 124.2, 122.8, 121.7, 121.5, 121.4,

120.4, 118.8, 114.2, 113.7, 108.7, 108.1, 55.3, 25.8, 25.7 ppm. Anal. Calcd for $C_{17}H_{15}NO_2$: C, 76.96; H, 5.70; N, 5.28; Found: C, 77.03; H, 5.77; N, 5.33.

1-Methyl-3-pyridin-4-ylmethylene-1,3-dihydro-indol-2-one (73) (KWC-I-84)

To a 4 dram vial was added 1-methyl-2-oxindole (**66**) (0.2107 g, 1.43 mmol), 4-pyridinecarboxaldehyde (161 μ L, 1.72 mmol, 1.2 equiv), piperidine (20 μ L, 0.210 mmol, 0.147 equiv) and EtOH (4 mL). The vial was heated at 90°C for 6 h while stirring. The mixture was allowed to cool to rt and was then placed in the freezer overnight. No precipitate formed so the solution was evaporated under reduced pressure to afford an orange oil which was subjected to column chromatography (70:30 Hexanes:EtOAc) to afford a yellow oil which was recrystallized with DCM/hexanes to afford a yellow solid (0.1794 g, 53.04%): mp 77-81°C; GC/MS (m/z) 236(M^+ , 100%): R_f = 0.20 (1:1 Hexanes/EtOAc); 1H NMR (300 MHz, DMSO- d_6) δ : 8.72 (dd, J = 1.59, 5.98 Hz, 2H), 8.66 (dd, J = 1.59, 6.11 Hz, 1H), 8.09 (dd, J = 1.54, 6.12, 1H), 7.78 (s, 1H, H-Vinyl), 7.74 (dd, J = 0.49, 8.01 Hz, 1H), 7.62-7.59 (m, 2H), 7.34-7.31 (m, 2H), 7.09-6.97 (m, 1H) 6.90 (dt, J = 0.99, 8.62 Hz, 1H) 3.18 (s, 3H, N-CH₃), 3.16 (s, 1H); ^{13}C NMR (75 MHz DMSO- d_6) δ : 166.6, 164.8, 150.1, 149.6, 144.4, 142.6, 142.1, 140.5, 133.3, 132.7, 130.8, 130.1, 129.6, 129.2, 124.6, 123.0, 122.5, 121.8, 120.2, 119.5, 109.0, 108.5, 26.0 ppm. Anal. Calcd for $C_{15}H_{12}N_2O$: C, 76.25; H, 5.12; N, 11.86; Found: C, 76.17; H, 5.06; N, 11.75.

3-(2,6-Difluoro-benzylidene)-1-methyl-1,3-dihydro-indol-2-one (74) (KWC-II-73)

To a 4 dram vial was added 1-methyl-2-oxindole (**66**) (0.3049 g 2.072 mmol), 2,6-difluorobenzaldehyde (268 μ L, 2.490 mmol, 1.2 equiv), piperidine (30 μ L, 0.304 mmol, 0.147 equiv) and EtOH (4 mL). The vial was heated at 90°C for 6 h while stirring. The mixture was allowed to cool to rt and placed in the freezer overnight. No precipitate formed so the solution was evaporated under reduced pressure to afford an orange oil which was subjected to column chromatography (70:30 hexanes:ethyl acetate) to afford an orange oil which was recrystallized with DCM/hexanes to afford a yellow solid (0.1619 g, 29%): mp 108-110°C; GC/MS (m/z) 271 (M^+ , 100%); R_f = 0.85 (1:1 Hexanes/EtOAc); ^1H NMR (300 MHz, DMSO- d_6) δ : 7.67-7.57 (m, 1H), 7.43 (s, 1H, H-vinyl), 7.37-7.33 (m, 1H), 7.29 (t, J = 8.13 Hz, 2H), 7.04 (d, J = 7.84 Hz, 1H), 6.94-6.93 (m, 2H), 3.21 (s, 3H, N-CH₃); ^{13}C NMR (75 MHz, DMSO- d_6) δ : 166.6, 161.8-161.7, 158.5-158.4, 144.8, 132.7-132.4, 131.8, 131.8, 123.2-123.2, 122.5, 120.8-120.8, 112.8-112.4, 109.4, 26.4 ppm. Anal. Calcd for C₁₆H₁₁F₂NO: C, 70.84; H, 4.09; N, 5.16; Found: C, 71.01; H, 3.93; N, 5.18.

1-Methyl-3-pyridin-2-ylmethylene-1,3-dihydro-indol-2-one (75) (KWC-I-86)

To a 4 dram vial was added 1-methyl-2-oxindole (**66**) (0.2181 g 1.48 mmol), 2-pyridinecarboxaldehyde (169.2 μ L, 1.78 mmol, 1.2 equiv), piperidine (21.5 μ L, 0.218 mmol, 0.147 equiv) and EtOH (4 mL). The vial was heated at 90°C for 6 h while stirring. The mixture was allowed to cool to rt and placed in the freezer overnight, after which a black precipitate (0.2509 g, 71.6%) was collected by vacuum filtration and washed with EtOH: mp 137-140°C; GC/MS (m/z) 236 (M^+ , 100%); R_f = 0.67 (1:1 Hexanes/EtOAc); ^1H NMR (300 MHz, DMSO- d_6) δ : 9.04 (d, J = 7.36, 1H), 8.89-8.87 (m, 1H), 7.97-7.86 (m,

2H), 7.64 (s, 1H, H-vinyl), 7.48-7.44 (m, 1H), 7.36 (dt, $J = 1.21, 7.68$ Hz 1H), 7.07-6.90 (m, 2H), 3.21 (s, 3H, N-CH₃); ¹³C NMR (75 MHz DMSO-*d*₆) δ : 167.8, 153.0, 149.6, 144.6, 137.1, 134.1, 130.7, 128.5, 128.3, 127.6, 124.1, 121.6, 120.9, 108.2, 26.0 ppm. Anal. Calcd for C₁₅H₁₂N₂O: C, 76.25; H, 5.12; N, 11.86; Found: C, 76.07; H, 5.22; N, 11.86.

3-(4-Chloro-benzylidene)-1-methyl-1,3-dihydro-indol-2-one (76) (KWC-I-88)

To a 4 dram vial was added 1-methyl-2-oxindole (**66**) (0.2283 g 1.59 mmol), 4-chlorobenzaldehyde (169.2 μ L, 1.78 mmol, 1.2 equiv), piperidine (23 μ L, 0.234 mmol, 0.147 equiv) and EtOH (4 mL). The vial was heated at 90°C for 4.5 h while stirring. The mixture was allowed to cool to rt and placed in the freezer overnight, after which time a yellow precipitate (0.2602 g) was collected by vacuum filtration and recrystallized with EtOH to afford (0.1000 g, 23.3%): mp 101-103°C; GC/MS: (m/z) 269(M⁺, 100%), R_f = 0.51, 0.67 (1:1 Hexanes/EtOAc); ¹H NMR (300 MHz, DMSO-*d*₆) δ 7.70 (d, $J = 8.22$ Hz, 2H), 7.65 (s, 1H, H-vinyl), 7.57 (d, $J = 8.42$, 2H), 7.52-7.48 (m, 1H), 7.32 (td, $J = 1.09, 7.74$ Hz, 1H), 7.03-7.00 (m, 1H), 6.91 (td, $J = 1.06, 7.64$ Hz 1H), 3.19 (s, 3H, N-CH₃); ¹³C NMR (75 MHz, DMSO-*d*₆): δ 167.5, 165.6, 144.6, 142.5, 135.8, 135.4, 135.3, 134.7, 134.0, 133.7, 133.2, 131.6, 130.8, 129.7, 129.3, 128.7, 127.7, 126.7, 124.1, 122.6, 122.19-122.16, 120.4, 120, 109.4, 108.8, 26.4, 26.3 ppm. Anal. Calcd for C₁₆H₁₂ClNO: C, 71.25; H, 4.48; N, 5.12; Found: C, 71.10; H, 4.52; N, 5.13.

3-(2,6-dichlorobenzylidene)-1-methyl-1,3-dihydro-indol-2-one (77) (KWC-I-89)

To a 4 dram vial was added 1-methyl-2-oxindole (**66**) (0.2064 g, 1.40 mmol), 2,6-dichlorobenzaldehyde (0.3003 g, 1.71 mmol, 1.2 equiv), piperidine (20.4 μ L, 0.206 mmol, 0.147 equiv) and EtOH (4 mL). The vial was heated at 90°C for 4.5 h while stirring. The mixture was allowed to cool to rt and placed in the freezer overnight, after which time a yellow precipitate (0.3353 g) was collected by vacuum filtration and recrystallized with EtOH to afford (0.2929 g, 68.8%): mp 168-171°C; GC/MS: (*m/z*) 303 (M^+), 268 (100%); R_f = 0.52 (1:1 Hexanes/EtOAc); ^1H NMR (300 MHz, DMSO- d_6) δ : 7.79 (ddd, J = 0.68, 1.54, 8.03 Hz, 1H), 7.72 (ddd, J = 0.78, 1.54, 7.75 Hz, 1H), 7.64 (s, 1H, H-vinyl), 7.55-7.50 (m, 1H), 7.35 (td, J = 1.19, 7.64 Hz, 1H), 7.10-7.05 (m, 2H), 6.89 (td, J = 1.13, 7.56 Hz, 1H), 3.22 (s, 3H); ^{13}C NMR (75 MHz, DMSO- d_6): 167.0, 144.8, 135.9, 132.9, 132.0, 131.8, 131.3, 131.1, 129.6, 129.4, 129.1, 122.9, 122.4, 120.1, 109.6, 26.5 ppm. Anal. Calcd for $\text{C}_{16}\text{H}_{11}\text{Cl}_2\text{NO}$: C, 63.18; H, 3.65; N, 4.60; Found: C, 63.16; H, 3.71; N, 4.72.

3-(2-Hydroxybenzyliden)-1-methyl-1,3-dihydro-indol-2-one (78) (KWC-I-90)

To a 4 dram vial was added 1-methyl-2-oxindole (**66**) (0.2081 g 1.41 mmol), salicylaldehyde (181.0 μ L, 1.69 mmol, 1.2 equiv), piperidine (21.0 μ L, 0.208 mmol, 0.147 equiv) and EtOH (4 mL). The vial was heated at 90°C for 4.5 h while stirring. The mixture was allowed to cool to rt and placed in the freezer overnight, after which time a yellow precipitate (0.3128 g) was collected by vacuum filtration and recrystallized with EtOH to afford (0.1870 g, 52.8 %): mp 209-212°C; GC/MS: (*m/z*) 251 (M^+), 234 (100%); R_f = 0.33 (1:1 Hexanes/EtOAc); ^1H NMR (300 MHz, DMSO- d_6) δ : 10.20 (s, 1H, -OH), 7.79 (s, 1H, H-vinyl), 7.62 (dd, J = 1.08, 7.58, 1H), 7.54 (d, J = 7.51, 1H), 7.35-7.26 (m,

2H), 7.00 (d, $J = 7.91$, 2H), 6.95-6.89 (m, 2H), 3.20 (s, 3H, N-CH₃); ¹³C NMR (75 MHz, DMSO-*d*₆) δ : 167.3, 156.5, 143.7, 133.0, 131.7, 129.6-129.5, 125.5, 122.0, 121.5, 121.2, 120.6, 118.8, 116.0, 108.6, 25.9 ppm. Anal. Calcd for C₁₆H₁₃NO₂: C, 76.48; H, 5.21; N, 5.57; Found: C, 76.77; H, 5.36; N, 5.70.

3-(3-Phenyl-2-propenylidene)-1-methyl-1,3-dihydro-indol-2-one (80) (KWC-I-91)

To a 4 dram vial was added 1-methyl-2-oxindole (**66**) (0.2399 g, 1.63 mmol), *trans*-cinnamaldehyde (246.2 μ L, 1.96 mmol, 1.2 equiv), piperidine (24 μ L, 0.239 mmol, 0.147 equiv) and EtOH (4 mL). The vial was heated at 90°C for 6 h while stirring. The mixture was allowed to cool to rt and placed in the freezer overnight, after which time a red precipitate (0.2024 g, 47.5%) was collected by vacuum filtration and recrystallized with EtOH to afford (0.1323 g, 31.1%): mp 162-164°C; GC/MS: (m/z) 261 (M⁺, 100%); R_f = 0.49 (1:1 Hexanes/EtOAc); ¹H NMR (300 MHz, DMSO-*d*₆) δ : 7.69-6.73 (m, 10H), 3.15 (s, 3H, N-CH₃) 3.02 (s, 6H, N(CH₃)₂). Anal. Calcd for C₁₈H₁₅NO: C, 82.73; H, 5.79; N, 5.36; Found: C, 82.96; H, 5.91; N 5.41.

3-(3-[4-(Dimethylamino)phenyl]-2-propenylidene-5-chloro-1,3-dihydro-indol-2-one (81) (KWC-II-66)

To a 4 dram vial was added 5-chloro-oxindole (**79**) (0.3144 g, 1.876 mmol), 4-(dimethylamino)cinnamaldehyde (0.3974 g, 2.268 mmol, 1.2 equiv), piperidine (27.2 μ L, 0.276 mmol, 0.147 equiv) and EtOH (4 mL). The vial was heated at 90°C overnight while stirring. The mixture was allowed to cool to rt and placed in the freezer overnight, after which time a red precipitate (0.2882 g, 47.3%) was collected by vacuum filtration and

recrystallized with EtOH (0.2882 g, 47.3%); mp 280-283°C; LC/MS: 325 ($M^+ + 1$); $R_f = 0.28$ (1:1 Hexanes/EtOAc). $^1\text{H NMR}$ (300 MHz, DMSO- d_6) δ : 10.81 (s, 1H, N-H), 7.69-6.73 (m, 10H), 3.02 (s, 6H, N(CH₃)₂). Anal. Calcd for C₁₉H₁₇ClN₂O: C, 70.26; H, 5.28; N, 8.62; Found: C, 70.10; H, 5.47; N, 8.64.

3-(3-[4-(Dimethylamino)phenyl]-2-propenylidene-6-chloro-1,3-dihydro-indol-2-one (82) (KWC-II-67)

To a 4 dram vial was added 6-chloro-2-oxindole (**60**) (0.3187 g, 1.902 mmol), 4-(dimethylamino)cinnamaldehyde (0.4069 g, 2.555 mmol, 1.2 equiv), piperidine (28 μL , 0.280 mmol, 0.147 equiv) and EtOH (4 mL). The vial was heated at 90°C for 24 h while stirring. The mixture was allowed to cool to rt and placed in the freezer overnight, after which time a dark red precipitate (0.0774) was collected by vacuum filtration and recrystallized with EtOH; mp 269-271°C; LC/MS: (m/z) 325 ($M^+ + 1$); $R_f = 0.43$; $^1\text{H NMR}$ (300 MHz, DMSO- d_6) δ : 10.65 (bs, 1H, N-H), 7.93 (d, $J = 8.20$ Hz, 1H), 7.65 (d, $J = 8.91$ Hz, 2H), 7.50-7.41 (m, 1H), 7.29 (dd, $J = 8.22, 13.39$ Hz, 2H), 7.00 (dd, $J = 2.01, 8.16$ Hz, 1H), 6.86 (s, 1H), 6.74 (d, $J = 9.0$ Hz, 2H), 3.01 (s, 6H); $^{13}\text{C NMR}$ (75 MHz, DMSO- d_6): 169.6, 151.9, 147.4, 143.2, 137.5, 132.5, 130.5, 125.0, 123.9, 122.1, 121.5, 121.2, 118.6, 112.3, 109.9, 40.2 ppm; Anal. Calcd for C₁₉H₁₇ClN₂O: C, 70.26; H, 5.28; N, 8.62; Found: C, 69.15; H, 5.20; N, 8.44.

3-(3-[4-(Dimethylamino)phenyl]-2-propenylidene-7-chloro-1,3-dihydro-indol-2-one (83) (KWC-II-33)

To a 4 dram vial was added 7-chloro-2-oxindole (**61**) (0.3562 g, 2.125 mmol), 4-(dimethylamino)cinnamaldehyde (0.4528 g, 2.584 mmol, 1.2 equiv), piperidine (40 μ L, 0.312 mmol, 0.147 equiv) and EtOH (4 mL). The vial was heated at 90°C for 7 h while stirring. The mixture was allowed to cool to rt and placed in the freezer overnight, after which time a dark purple precipitate (0.5139 g, 74.4%) was collected by vacuum filtration and ran what would dissolve in DCM through a silica gel column (70:30 hexanes:EtOAc) to afford a dark purple solid (0.0545 g, 7.9%); mp 243-245°C; LC/MS: (*m/z*) 325 (M^+ +1); R_f = 0.47 (1:1 Hexanes/EtOAc); ^1H NMR (300 MHz, DMSO-*d*₆) δ : 10.80 (bs, 1H), 7.91 (d, J = 7.01 Hz, 1H), 7.66 (d, J = 8.94 Hz, 2H), 7.53-7.44 (m, 2H), 7.38-7.34 (m, 1H), 7.29-7.22 (m, 1H), 7.01 (dd, J = 7.72, 8.06 Hz, 1H), 6.75 (d, J = 8.97 Hz, 2H), 3.01 (m, 6H); ^{13}C NMR (75 MHz, DMSO-*d*₆) δ : 169.4, 168.8, 152.0, 151.9, 148.0, 145.9, 139.6, 139.1, 138.6, 137.9, 130.6, 129.9, 127.9, 127.6, 125.1, 124.0, 123.8, 122.8, 122.4, 122.3, 121.8, 121.5, 119.5, 118.4, 118.1, 114.2, 114.1, 112.6, 112.3, 40.2 ppm. Anal. Calcd for C₁₉H₁₇ClN₂O: C, 70.26; H, 5.28; N, 8.62; Found: C, 70.27; H, 5.26; N, 8.56.

3-(3-[4-(Dimethylamino)phenyl]-2-propenylidene-1-methyl-1,3-dihydro-indol-2-one (84) (KWC-II-36)

To a 4 dram vial was added 1-methyl-2-oxindole (**66**) (0.3021 g, 2.053 mmol), 4-(dimethylamino)cinnamaldehyde (0.4476 g, 2.554 mmol, 1.2 equiv), piperidine (22.2 μ L, 0.302 mmol, 0.147 equiv) and EtOH (4 mL). The vial was heated at 90°C for 7 h while stirring. The mixture was allowed to cool to rt and placed in the freezer overnight. No precipitate formed so the solution was evaporated under reduced pressure to afford a dark

oil which was subjected to column chromatography (70:30 Hexanes/EtOAc) to afford an oil which was recrystallized with DCM/hexanes to afford a brick red solid (0.1973 g, 31.6 %): mp 159-161°C; LC/MS: (*m/z*) 305 ($M^+ + 1$); $R_f = 0.44$ (1:1 Hexanes/EtOAc); ^1H NMR (300 MHz, DMSO-*d*₆) δ : 8.26 (dd, $J = 11.67, 15.50$ Hz, 0.4H), 7.96 (dd, $J = 0.18, 7.35$ Hz, 1H), 7.64 (d, $J = 8.91$ Hz, 1H), 7.58-7.50 (m, 1H), 7.46-7.42 (m, 1H), 7.36 (d, $J = 12.22$, 1H), 7.30-7.27 (m, 1H), 7.25-7.20 (m, 1H), 7.13-7.07 (m, 1H), 7.05-6.95 (m, 2H) 6.81-6.72 (m, 2H), 3.18(s, 3H), 3.00 (d, $J = 4.01$, 6H). Anal. Calcd for C₂₀H₂₀N₂O: C, 78.29; H, 6.62; N, 9.20; Found: C, 78.68; H, 6.51; N 9.17.

**3-(3-[4-(Dimethylamino)phenyl]-2-propenylidene-1,3-dihydro-indol-2-one (85)
(KWC-I-100)**

To a 4 dram vial was added oxindole (86) (0.2840 g, 2.133 mmol), 4-(dimethylamino) cinnamaldehyde (0.4613 g, 2.633 mmol, 1.2 equiv), piperidine (31 μL , 0.313 mmol, 0.147 equiv) and EtOH (4 mL). The vial was heated at 90°C for 6 h while stirring. The mixture was allowed to cool to rt and placed in the freezer overnight, after which time a red precipitate (0.1038 g, 16.8%) was collected by vacuum filtration and recrystallized with EtOH (0.0796 g, 13%) and again with EtOH (0.0284 g, 5%): mp 230-234°C; GC/MS: (*m/z*) 261 (M^+), M^+ (100%); $R_f = 0.57$ (1:1 Hexanes/EtOAc). ^1H NMR (300 MHz, DMSO-*d*₆) δ : 10.75 (s, 1H, N-H), 7.68-6.71 (m, 11H), 3.01 (s, 6H, N(CH₃)₂) Anal. Calcd for C₁₉H₁₈N₂O: C, 78.59; H, 6.25; N, 9.65; Found: C, 78.49; H, 6.30; N 9.70.

References

- 1) Scifinder Scholar. *Alzheimer's Disease*.
<https://scifinder.cas.org/scifinder/view/scifinder/scifinderExplore.jsf> (accessed July, 14, 2014).
- 2) Stelzmann R.A.; Schnitzlein H.N.; Murtagh, F.R. An English Translation of Alzheimer's 1907 Paper, "Uber eine eigenartige Erkankung der Hirnrinde" *Clin. Anat.* **1995**, *8*, 429-431
- 3) Graeber, M.B.; Kosel, S.; Egensperger, R.; Banati, R.B.; Muller, U.; Bise, K.; Hoff, P.; Moller, H.J.; Fujisawa, K.; Mehraein, P. "Rediscovery of the case by Alois Alzheimer in 1911: historical, histological and molecular genetic analysis" *Neurogenetics* **1997**, *1*, 73-80
- 4) O'Brian, C. "Auguste D. and Alzheimer's disease." *Science* **1996**, *273*, 28-?
- 5) Graeber, M.B.; Mehraein P. "Reanalysis of the first case of Alzheimer's disease" *Eur. Arch. Psychiatry Clin. Neurosci.* **1999**, *249*, 11-13
- 6) Amaducci, L. "Alzheimer's original patient" *Science* **1996**, *274*:328
- 7) Amaducci, L.; Sorbi, S.; Piacentini, S.; Bick, K.L. "The first Alzheimer disease case: A metachromatic leukodystrophy" *Dev. Neurosci.* **1991**, *13*, 186-187
- 8) Alzheimer's Association. "2012 Alzheimer's disease facts and figure" *Alzheimers Dement.* **2012**, *8*, 131-168.
- 9) Herbert, L.E.; Weuve, J.; Scherr P.A.; Evans, D.A. "Alzheimer disease in the United States (2010-2050) estimated using the 2010 census" *Neurology.* **2013**, *80*, 1778-1783

- 10) Hardy, J.A.; Higgins, G.A. "Alzheimer's Disease: The Amyloid Cascade Hypothesis" *Science* **1992**, *256*, 184-185.
- 11) Lichtenthaler, S.F.; Wang, R.; Grimm, H.; Uljon, S.N.; Masters, C.L.; Beyreuther, K. "Mechanism of the cleavage specificity of Alzheimer's disease γ -secretase identified by phenylalanine-scanning mutagenesis of the transmembrane domain of the amyloid precursor protein" *Proc. Natl. Acad. Sci. USA* **1999**, *96*, 3053-3058
- 12) Hardy J.; Selkoe D.J. "The Amyloid Hypothesis of Alzheimer's Disease: Progress and Problems on the Road to Therapeutics" *Science* **2002**, *297*, 353-356
- 13) Wang, J.; Dickson, D.W.; Trojanowski, J.Q.; Lee, V.M.-Y. "The Levels of Soluble versus Insoluble Brain AB Distinguish Alzheimer's Disease from Normal and Pathologic Aging" *Exp. Neurol.* **1999**, *158*, 328-337
- 14) Citron, M.; Westaway, D.; Xia, W.; Carlson, G.; Diehl, T.; Levesque, G.; Johnson-Wood, K.; Lee, M.; Seubert, P.; Davis, A.; Kholodenko, D.; Motter, R.; Sherrington, R.; Perry, B.; Yao, H.; Stroma, R.; Lieberburg, I.; Rommens, J.; Kim, S.; Schenk, D.; Fraser, P.; Hyslop, P.; Selkoe, D.J. "Mutatant presenilins of Alzheimer's disease increase production of 42-residue amyloid β -protein in both transfected cells and transgenic mice" *Nature Med.* **1997**, *3*, 67-72
- 15) Mehta, N.D.; Refolo, L.M.; Eckman, C.; Sanders, S.; Yager, D.; Perez-Tur, J.; Younkin, S.; Duff, K.; Hardy, J.; Hutton, M. "Increase A β 42(43) from Cell Lines Expressing Presenilin 1 Mutations" *Ann. Neurol.* **1998**, *43*, 256-258
- 16) Houlden, H.; Baker, M.; McGowan, E.; Lewis, P.; Hutton, M. Crook, R.; Wood, N.W.; Kumar-Singh, S.; Geddes, J.; Swash, M.; Scaravilli, F.; Holton, J.L.; Lashley, T.; Tomita, T.; Hashimoto, T.; Verkkoniemi, A.; Kalimo, H.; Somer, M.;

- Paetau, A.; Martin, J.J.; Broeckhoven, C.V.; Golde, T.; Hardy, J.; Haltia, M.; Revesz, T. "Variant Alzheimer's Disease with Spastic Paraparesis and Cotton Wool Plaques Is Caused by PS-1 Mutations that Lead to Exceptionally High Amyloid- β Concentrations" *Ann. Neurol.* **2000**, 48, 806-808
- 17) Smith, M.J.; Kwok, J.B.J.; McLean, C.A.; Krill, J.J.; Broe, G.A.; Nicholson, G.A.; Cappai, R.; Hallupp, M.; Cotton, R.G.H.; Masters, C.L.; Schofield, P.R.; Brooks, W.S. "Variable Phenotype of Alzheimer's Disease with Spastic Paraparesis" *Ann. Neurol.* **2001**, 49, 125-129
- 18) Van Broeckhoven, C.; Backhovens, H.; Cruts, M.; Martin, J.J.; Crook, R.; Houlden, H.; Hardy, J. "APOE genotype does not modulate age of onset in families with chromosome 14 encode Alzheimer's Disease" *Neurosci. Lett.* **1994**, 169, 179-180
- 19) Games, D.; Adams, D.; Alessandrini, R.; Barbour, R.; Berthelette, P.; Blackwell, C.; Carr, T.; Clemens, J.; Donaldson, T.; Gillespie, F.; Guldo, T.; Hagopian, S.; Johnson-Wood, K.; Khan, K.; Lee, M.; Lelbowski, P.; Lieberburg, I.; Little, S.; Masliah, E.; McConlogue, L.; Montoya-Zavala, M.; Mucke, L.; Paganini, L.; Penniman, E.; Power, M.; Schenk, D.; Seubert, P.; Snyder, B.; Soriano, F.; Tan, H.; Vitale, J.; Wadsworth, S.; Wolozin, B.; Zhao, J. "Alzheimer-type neuropathology in transgenic mice overexpressing V717F β -amyloid precursor protein" *Nature* **1995**, 373, 523-527
- 20) Hsiao, K.; Chapman, P.; Nilsen, S.; Eckman, C.; Harigaya, Y.; Younkin, S.; Yang, F.; Cole, G. "Corrective Memory Deficits, A β Elevation, and Amyloid Plaques in Transgenic Mice" *Science* **1996**, 274, 99-102

- 21) Irizarry, M.; Ferdie, S.; McNamare, M.; Page, K.J.; Schenk, D.; Games, D.; Hyman, B.T. "A β Deposition Is Associated with Neuropil Changes, but not with Overt Neuronal Loss in the Human Amyloid Precursor Protein V717F (PDAPP) Transgenic Mouse" *J. Neurosci.* **1997**, 17, 7053-7059
- 22) Lewis, J.; Dickson, D.W.; Lin, W-L.; Chisholm, L.; Corral, A.; Jones, G.; Yen, S-H.; Sahara, N.; Skipper, L.; Yager, D.; Eckman, C.; Hardy, J.; Hutton, M.; McGowan, E. "Enhanced Neurofibrillary Degeneration in Transgenic Mice Expressing Mutant Tau and APP" *Science* **2001**, 293, 1487-1491
- 23) Braak, H.; Braak, E. "Neuropathological staging of Alzheimer-related changes" *Acta. Neuropathol.* **1991**, 82, 239-259
- 24) Mann, D.M.A.; Yates, P.O.; Marcyniuk, B. Ravindra, C.R. "The Topography of Plaques and Tangles in Down's Syndrome Patients of Different Ages" *Neuropathol. App. Neurobiol.* **1986**, 12, 447-457
- 25) Lemere, C.A.; Blusztajn, J.K.; Yamaguchi, H. Wisniewski, T.; Saido, T.C.; Selkoe, D.J. "Sequence of Deposition of Heterogeneous Amyloid β -Peptides and APO E in Down Syndrome: Implications for Initial Events in Amyloid Plaque Formation" *Neurobiol. Dis.* **1996**, 3, 16-32
- 26) Fitzgerald, S. "Two Large Alzheimer's Trail Fail to Meet Endpoints: What's Next?" *Neurol. Today*, 6 March, 2014: 12-15. Print
- 27) Klunk, W.E.; Debnath, M.L.; Pettegrew, J.W. "Development of Small Molecule Probes for the Beta-Amyloid Protein of Alzheimer's Disease" *Neurobiol. Aging* **1994**, 15, 691-698

- 28) Mathis, C.A.; Wang, Y.; Holt, D.P.; Huang, G.; Debnath, M.L.; Klunk, W.E.
“Synthesis and Evaluation of ^{11}C -Labeled 6-Substituted 2-Arylbenzothiazoles as
Amyloid Imaging Agents” *J. Med. Chem.* **2003**, 46, 2740-2754
- 29) Dishino, D.D.; Welch, M.J.; Kilbourn, M.R.; Raichle, M.E.; “Relationship
between lipophilicity and brain extraction of C-11-labeled radiopharmaceuticals”
J. Nucl. Med. **1983**, 24, 1030-1038
- 30) Pike, V.W.; McCarron, J.A.; Lammertsma, A.A.; Osman, S.; Hume, S.P.; Sargent,
P.A.; Bench, C.J.; Cliffe, I.A.; Fletcher, A.; Grasby, P.M. “Exquisite delineation
of 5-HT_{1A} receptors in human brain with PET and [carbonyl- ^{11}C]WAY-100635”
Euro. J. Pharmacol. **1996**, 301, R5-7.
- 31) Drevets, W.C.; Frank, E.; Price, J.C.; Kupfer, D.J.; Holt, D.; Greer, P.J.; Huang,
Y.; Gautier, C.; Mathis, C. “PET imaging of serotonin 1A receptor binding in
depression. *Biol. Psych.* **1999**, 46, 1375-1387.
- 32) Farde, L.; Halldin, C.; Stone-Elander, S.; Sedvall, G. “PET Analysis of human
dopamine receptor subtypes using ^{11}C -SCH23390 and ^{11}C -raclopride.
Psychopharmacology (Berl.) **1987**, 92, 278-284
- 33) Farde, L.; Pauli, S.; Hall, H.; Eriksson, L.; Halldin, C.; Hogberg, T.; Nilsson, L.;
Sjogren, I.; Stone-Elander, S. “Stereoselective binding of ^{11}C -raclopride in living
human brain – a search for extrastriatal central D₂-dopamine receptors by PET.
Psychopharmacology (Berl.) **1988**, 94, 471-478.
- 34) Smith, G.S.; Price, J.C.; Lopresti, B.J.; Haung, Y.; Holt, D.; Mason, N.S.;
Simpson, N.R.; Sweet, R.; Meltzer, C.C.; Sashin, D.; Mathis, C.A.; “Test-retest
variability of serotonin 5-HT_{2A} receptor binding measured with positron

- emission tomography (PET) and [F-18]altanserin in the human brain” *Synapse* **1998**, *30*, 380-392
- 35) Price, J.C.; Lopresti, B.J.; Mason, N.S.; Holt, D.P.; Meltzer, C.C.; Smith, G.S.; Gunn, R.N.; Huang, Y.; Mathis, C.A. “Analyses of [¹⁸F]altanserin bolus injection PET date II: consideration of radiolabeled metabolites in humans” *Synapse* **2001**, *41*, 11-21
- 36) Lopresti, B.J.; Mathis, C.A.; Price, J.C.; Villemagne, V.L.; Meltzer, C.C.; Holt, D.P.; Smith, G.S.; Moore, R.Y.; “Serotonin transporter binding in vivo: further examination of [¹¹C]-McN5652, In *Molecular and Pharmacological Brain Imaging with Positron Emission Tomography*; Gjedde A., Ed.; Academic Press: San Diego, 2001; pp 265-271
- 37) Huang, Y.; Hwang, D.R.; Narendran, R.; Sudo, Y.; Chatterjee, R.; Bae, S.A.; Mawlawi, O.; Kegeles, L.S.; Wilson, A.A.; Kung, H.F.; Laruelle, M. “Comparative evaluation in nonhuman primates of five PET radiotracers for imaging the serotonin transporters: [¹¹C]McN5652, [¹¹C]ADAM, [¹¹C]DASB, [¹¹C]DAPA, and [¹¹C]AFM. *J. Cereb. Blood Flow Metab.* **2002**, *22*, 1377-1398.
- 38) Engler, H.; Blomqvist, G.; Bergstrom, M.; Langstrom, B.; Klunk, W.; Debnath, M.; Holt, D.; Wang, Y.; Huang, G.-F.; Mathis, C. “First human study with a benzothiazole amyloid-imaging agent in Alzheimer’s disease and control subjects. *Neurobiol. Aging* **2002**, *23* (Suppl.) S1568
- 39) Klunk, W.E.; Engler, H.; Nordberg, A.; Wang, Y.; Blomqvist, G.; Holt, D.P.; Bergstrom, M.; Savitcheva, I.; Huang, G.-F.; Estrade, S.; Ausen, B.; Debnath, M.L.; Barletta, J.; Price, J.C.; Sandell, J.; Lopresti, B.J.; Wall, A.; Koivisto, P.;

- Antoni, G.; Mathis, C.A.; Langstrom, B.; "Imaging brain amyloid in Alzheimer's disease with Pittsburgh Compound-B" *Ann. Neurol.* **2004**, *55*, 306-319
- 40) Klunk, H.F.; Lee, C.-W.; Zhuang, Z.-P.; Kung, M.-P.; Hou, C.; Plossl, K. "Novel stilbenes as probes for amyloid plaques" *J. Am. Chem. Soc.* **2001**, *123*, 12740-12741
- 41) Kung, H.F.; Choi, S.R.; Qu, W.; Zhang, W.; Skovronsky, D. "¹⁸F Stilbenes and Styrylpyridines for PET Imaging of AB Plaques in Alzheimer's Disease: A Miniperspective" *J. Med. Chem.* **2010**, *53*, 933-941
- 42) Zhang, W.; Kung, M.P.; Oya, S.; Hou, C.; Kung, H.K. "(¹⁸F)-Labeled styrylpyridines as PET agents for amyloid plaques imaging" *Nucl. Med. Biol.* **2007**, *34*, 89-97
- 43) Zhang, W.; Oya, S.; Klunk, M.P.; Hou, C.; Mauer, D.L.; Kung, H.F. "F-18 Polyethyleneglycol stilbenes as PET imaging agents targeting A β aggregates in the brain" *Nucl. Med. Biol.* **2005**, *32*, 799-809
- 44) Stephenson, K.A.; Chandra, R.; Zhuang, Z.-P.; Hou, C.; Oya, S.; Hung, M.-P.; Kung, H.F. "Fluro-pegylated (FPEG) imaging agents targeting A β aggregates" *Bioconjugate Chem.* **2001**, *18*, 238-246
- 45) Pardridge, W.M. "Molecular biology of the blood-brain barrier" *Mol. Biotechnol.* **2005**, *30*, 57-70
- 46) Rowe, C.C.; Ackerman, U.; Browne, W.; Mulligan, R.; Pike, K.L.; O'Keefe, G.; Tochon-Danguy, H.; Chan, G.; Berlangieri, S.U.; Jones, G.; Dickinson-Rowe, K.L.; Kung, H.P.; Zhang, W.; Kung, M.P.; Skovronsky, D.; Dyrks, T.; Holl, G.; Krause, S.; Friebe, M.; Lehman, L.; Lindemann, S.; Dinkelborg, L.M.; Masters,

- C.L.; Villemagna, V.L. “Imaging of amyloid beta in Alzheimer’s disease with (18)F-BAY94-9172, a novel PET tracer: proof of mechanism” *Lancet Neurol.* **2008**, 7, 129-135
- 47) a) Ballatore, C.; Lee, V. M.-Y.; Trojanowski, J.Q. “Tau-mediated neurodegeneration in Alzheimer’s disease and related disorders” *Nature Rev. Neurosci.* **2007**, 8, 663-672
- b) Brunden, K.R.; Trojanowski, J.Q.; Lee, V.M.-Y. “Advances in tau-focused drug discovery for Alzheimer’s disease and related tauopathies” *Nature Rev. Neurosci.* **2009**, 8, 783-789
- 48) Lee, G.; Neve, R.L.; Kosik, K.S. “The microtubule binding domain of tau protein” *Neuron.* **1989**, 2, 1615-1624
- 49) Binder, L.I.; Frankfurter, A. Rebhun, L.I. “The distribution of tau in the mammalian central nervous system” *J. Cell Biol.* **1985**, 101, 1371-1378
- 50) Hong, M. *et al.* “Mutation-specific functional impairments in distinct tau isoforms of hereditary” *Science*, **1998**, 282, 1914-1917
- 51) Forman, M.S.; Trojanowski, J.Q.; Lee, V.M.-Y. “Neurodegenerative diseases: A decade of discoveries paves the way for therapeutic breakthroughs” *Nature*, **2004**, 10, 1055-1063
- 52) Trojanowski, J.Q.; Mattson, M.P. “Overview of protein aggregation in single, double, and triple neurodegenerative brain amyloidosis” *Neuromolecular Med.* **2003**, 4, 1-6

- 53) Mitchell, T.W. *et al.* “Novel method to quantify neutrophil threads in brains from elders with or without cognitive impairment” *J. Histochem. Cytochem.* **2000**, *48*, 1627-1638
- 54) Roy, S.; Zhang, B.; Lee, V.M.-Y.; Trojanowski, J.Q. “Axonal transport defects: a common theme in neurodegenerative diseases” *Acta Neuropathol.* **2005**, *109*, 5-13
- 55) Trojanowski, J.Q.; Smith, A.B.; Hurn, D.; Lee, V.M.-Y. “Microtubule-stabilizing drugs for therapy of Alzheimer’s disease and other neurodegenerative disorders with axonal transport impairments” *Expert Opin. Pharmacother.* **2005**, *6*, 683-686
- 56) Ishihara, T. *et al.* “Age-dependent emergence and progression of a tauopathy in transgenic mice overexpressing the shortest human tau isoform” *Neuron* **1999**, *24*, 751-762
- 57) Zhang, B. *et al.* “Microtubule-binding drugs offset tau sequestration by stabilizing microtubules and reversing fast axonal transport deficits in a tauopathy model” *Proc. Natl. Acad. Sci.* **2005**, *102*, 227-231
- 58) Arriagade, P.V.; Growdon, J.H.; Hedley-Whyte, E.T.; Hyman, B.T. “Neurofibrillary tangles but not senile plaques parallel duration and severity of Alzheimer’s disease” *Neurology* **1992**, *42*, 631-639
- 59) Arriaga, P.V.; Marzloff, K.; Hyman, B.T. “Distribution of Alzheimer-type pathologic changes in nondemented elderly individuals matches the pattern in Alzheimer’s disease” *Neurology* **1992**, *42*, 1681-1688

- 60) Honson, N.S.; Johnson, R.L.; Huang, W.; Inglese, J.; Austin, P.; Kuret, J.
“Differentiating Alzheimer disease-associated aggregates with small molecules”
Neurobiol. Dis. **2007**, 28, 251-260
- 61) Mena, R. “Monitoring Pathological assembly of tau and beta amyloid proteins in
Alzheimer’ disease.” *Acta Neuropathol.* **1995**, 89, 50-56
- 62) Caprathe, B.W. “Method of imaging amyloid deposits.” *U.S. Patent 6,001,331.*
1999
- 63) Wischik, C.M., et al., 2004. “Neurofibrillary labels” *U.S. Patent Application*
0213736 A1
- 64) Jensen, J.R.; Cisek, K.; Funk, K.E.; Naphade, S.; Schafer, K.N.; Kuret, J.
“Research Towards Tau Imaging” *J. Alzheimer Dis.* **2011**, 26, 147-157
- 65) Chirita, C.N. “Anionic Micelles and Vesicles Induce Tau Fibrillation *in vitro*” *J.*
Biol. Chem. **2003**, 278, 25644-25650
- 66) Hargreaves, R.J. “It Ain’t Over ‘til It’s Over”-The Search for Treatment and
Cures for Alzheimer’s Disease *ACS Med. Chem. Lett.* **2012**, 3, 862-866
- 67) U.S. Food and Drug Administration. *FDA approves imaging drug Amyvid*
<http://www.fda.gov/newsevents/newsroom/pressannouncements/ucm299678.htm>
(accessed August 25, 2014).
- 68) Okamura, N.; Furumoto, S.; Harada, R.; Tago, T.; Yoshikawa, T.; Fodero-
Tavoletti, M.; Mulligan, R.S.; Villemagna, V.L.; Akatsu, H.; Yamamoto, T.; Arai,
H.; Iwata, R.; Yanai, K.; Kudo, Y. “Novel ¹⁸F-labeled arylquinoline derivatives
for noninvasive imaging of tau pathology in Alzheimer disease” *J. Nucl. Med.*
2013, 54, 1420-1427

- 69) Chien, D.T.; Bahri, S.; Szardenings, A.K.; Walsh, J.C.; Mu, F.; Su, M.-Y.; Shankle, W.R.; Elizarov, A.; Kolb, H.C. “Early clinical PET imaging results with the novel PHF-tau radioligand [F-18]-T807” *J. Alzheimers Dis.* **2013**, *34*, 457-468
- 70) Chien, D.T.; Szardenings, A.K.; Bahri, S. Walsh, J.C.; Mu, F.; Xia, C.; Shankle, W.R.; Lerner, A.J.; Su, M.-Y.; Elizarov, A.; Kolb, H.; “Early clinical PET imaging results with the novel PHF-tau radioligand [F-18]-T808” *J. Alzheimers Dis.* **2014**, *38*, 171-184
- 71) Mathis, C.A.; Klunk, W.; “Imaging tau deposits in vivo: progress in viewing more of the proteopathy picture” *Neuron* **2013**, *79*, 1035-1037
- 72) Maruyama, M.; Shimada, H.; Suhara, T.; Shinotoh, H.; Ji, B.; Maeda, J.; Zhang, M.-R.; Trojanowski, J.Q.; Lee, V.M.-Y.; Ono, M.; Masamoto, K.; Takano, H.; Sahara, N.; Iwata, N.; Okamura, N.; Furumoto, S.; Kudo, Y.; Chang, Q.; Saido, T.C.; Takashima, A.; Lewis, J.; Jang, M.-K.; Aoki, I.; Ito, H.; Higuchi, M. “Imaging of tau pathology in a tauopathy mouse model and in Alzheimer patients compared to normal controls” *Neuron* **2013**, *79*, 1094-1108
- 73) Sun, L.; Tran, N.; Tang, F.; App, H.; Hirth, P.; McMahon, G.; Tang, C. “Synthesis and biological evaluations of 3-substituted indolin-2-ones: a novel class of tyrosine kinase inhibitors that exhibit selectivity toward particular receptor tyrosine kinases” *J. Med. Chem.* **1998**, *41*, 2588-2603.
- 74) Mosconi, L.; Tsui, W.H.; Herholz, K.; Pupi, A.; Drzezga, A.; Lucignani, G.; Reiman, E.M.; Holthoff, V.; Kalbe, E.; Sorbi, S.; Diehl-Schmid, J.; Perneczky, R.; Clerici, F.; Caselli, R.; Beuthien-Bauman, B.; Kurz, A.; Minoshima, S.; de Leon, M.J. “Multicenter Standardized ¹⁸F-FDG PET Diagnosis of Mild Cognitive

- Impairment, Alzheimer's Disease, and Other Dementia" *J Nucl Med.* **2008**, 49, 390-398
- 75) Sumpter, W.C. "The Chemistry of Oxindole." *Chem Rev.* **1945**, 443
- 76) Wenkert, E.; Bhattacharyya, N.K.; Reid, T.L.; Stevens, T.E. "Alkylation of oxindoles" **1956**, 78, 797-801
- 77) Clay, C. M., Abdallah, H. M.; Jordan, C.; Knisley, K.; Ketcha, D. M. *ARKIVOC* **2012** (vi) 317-325.
- 78) Charles M. Clay, "Synthesis of Isatin Derivatives Used for the Inhibition of Pro-Apoptotic Jurkat T Cells", WSU Master's Thesis 2011
- 79) Kyle Knisley, "Libraries for Libraries Approach to the Synthesis of Arylidene Oxindoles", WSU Master's Thesis 2013.
- 80) Paul J. Repasky, "Novel Trisubstituted Arylidene Oxindoles with Potent Anti-Apoptotic Properties", WSU Master's Thesis 2011.
- 81) Shmidt, M.S.; Reverdito, A.M.; Kremenchuzky, L.; Perillo, I.A.; Blanco, M.M. "Simple and efficient microwave assisted *N*-alkylation of isatin" *Molecules*, **2008**, 13, 831-840
- 82) Chen, G.; Wang, Y.; Hao, X.; Mu, S.; Sun, Q. "Simple isatin derivatives as free radical scavengers: Synthesis, biological evaluation and structure-activity relationship" *Chem. Cent. J.* **2011**, 5, 1-5
- 83) Azizian, J.; Fallah-Bagher-Shaidaei, H.; Kefayati, H. "Simple and efficient microwave for the preparation of *N*-alkyl isatins under microwave irradiation" *Synth. Commun.* **2003**, 33, 789-793

- 84) Yamawaki, J.; Ando, T. "Potassium fluoride on inorganic solid supports. A search for further efficient reagents promoting hydrogen-bond-assisted alkylations" *Chem. Lett.* **1979**, *7*, 755-758.
- 85) Chiyanzu, I.; Hansell, E.; Gut, J.; Rosenthal, P. J.; McKerrow, J. H.; Chibale, K. "Synthesis and evaluation of isatins and thiosemicarbazone derivatives against cruzain, falcipain-2, and rhodesain" *Bioorg. Med. Chem. Lett.* **2003**, *13*, 3527-3530.
- 86) Todd, D. The Wolff-Kishner Reduction, in "Org. Reactions"; John Wiley and sons, Inc., New York, 1948; 378-422
- 87) Doyle, M.P.; Shanklin, M.S.; Pho, H.Q.; Mahapatro, S. "Rhodium (II) acetate and nafion-H catalyzed decomposition of *N*-aryldiazoamides. An efficient synthesis of 2(3*H*)-indolinones" *J. Org. Chem.* **1988**, *53*, 1017-1022
- 88) Luehr, G.W.; Jain, R.; Renslo, A.; Josyula, V.P.V.N.; Gordeev, M.F. **2006**. "Oxazolidinones containing oxindoles as antibacterial agents" *U.S. Patent*. US2006/0030609A1
- 89) Zhang, W.; Go, M. L. "Functionalized 3-benzylidene-indolin-2-ones: Inducers of NAD(P)H-quinone oxidoreductase 1 (NQO1) with antiproliferative activity" *Bioorg. Med. Chem.* **2009**, *17*, 2077-2090.
- 90) Coda, A.C.; Invernizzi, A.G.; Righetti, P.P.; Tacconi, G.; Gatti, G. "(*Z*)- and (*E*)-Arylidene-1,3-dihydroindol-2-ones: configuration, conformation, and infrared carbonyl stretching frequencies" *J. Chem. Soc. Perkin Trans. II* **1984**, *4*, 615-619.
- 91) Sigmaaldrich.com, (2015). *1-Methylisatin 97%* | *Sigma-Aldrich*. [online]
Available at:

[http://www.sigmaaldrich.com/catalog/product/aldrich/183075?lang=en®ion=](http://www.sigmaaldrich.com/catalog/product/aldrich/183075?lang=en®ion=US)
US [Accessed 8 Jan. 2015].